

Accelerated Article Preview

Neoadjuvant immunotherapy in mismatch-repair-proficient colon cancers

Received: 23 January 2025

Accepted: 24 September 2025

Accelerated Article Preview

Published online: 20 October 2025

Cite this article as: Tan, P. B. et al.

Neoadjuvant immunotherapy in mismatch-repair-proficient colon cancers. *Nature*
<https://doi.org/10.1038/s41586-025-09679-4>
(2025)

Pedro B. Tan, Yara L. Verschoor, José G. van den Berg, Sara Balduzzi, Niels F. M. Kok, Marieke E. Ijsselsteijn, Kat Moore, Adham Jurdì, Antony Tin, Paulien Kaptein, Monique E. van Leerdam, John B. A. G. Haanen, Emile E. Voest, Noel F. C. C. de Miranda, Ton N. Schumacher, Lodewyk F. A. Wessels & Myriam Chalabi

This is a PDF file of a peer-reviewed paper that has been accepted for publication. Although unedited, the content has been subjected to preliminary formatting. Nature is providing this early version of the typeset paper as a service to our authors and readers. The text and figures will undergo copyediting and a proof review before the paper is published in its final form. Please note that during the production process errors may be discovered which could affect the content, and all legal disclaimers apply.

1 **Neoadjuvant immunotherapy in mismatch-repair-proficient colon**
2 **cancers**

3
4 Pedro B. Tan^{1,13}, Yara L. Verschoor^{1,13}, José G. van den Berg², Sara Balduzzi³, Niels F.M. Kok⁴, Marieke
5 E. Ijsselsteijn⁵, Kat Moore⁶, Adham Jurdij⁷, Antony Tin⁷, Paulien Kaptein⁸, Monique E. van Leerdam^{1,9},
6 John B. A. G. Haanen^{8,10}, Emile E. Voest^{8,11}, Noel F. C. C. de Miranda⁵, Ton N. Schumacher^{8,11,12},
7 Lodewyk F. A. Wessels^{6,11}, Myriam Chalabi^{1,10}

8
9 ¹Department of Gastrointestinal Oncology, Netherlands Cancer Institute, Amsterdam, the Netherlands

10 ²Department of Pathology, Netherlands Cancer Institute, Amsterdam, the Netherlands

11 ³Department of Biometrics, Netherlands Cancer Institute, Amsterdam, the Netherlands

12 ⁴Department of Surgery, Netherlands Cancer Institute, Amsterdam, the Netherlands

13 ⁵Department of Pathology, Leiden University Medical Center, Leiden, the Netherlands

14 ⁶Department of Molecular Carcinogenesis, Netherlands Cancer Institute, Amsterdam, the Netherlands

15 ⁷Natera, Inc, Austin, TX, USA

16 ⁸Department of Molecular Oncology and Immunology, Netherlands Cancer Institute, Amsterdam, the Netherlands

17 ⁹Department of Gastroenterology and Hepatology, Leiden University Medical Center, Leiden, the Netherlands

18 ¹⁰Department of Medical Oncology, Netherlands Cancer Institute, Amsterdam, the Netherlands

19 ¹¹Oncode Institute, Utrecht, the Netherlands

20 ¹²Department of Hematology, Leiden University Medical Center, Leiden, the Netherlands

21 ¹³These authors contributed equally: Pedro B. Tan, Yara L. Verschoor

22
23

24 **Abstract**

25 Immune checkpoint blockade (ICB) has led to paradigm shifts in the treatment of various tumour
26 types¹⁻⁴, yet limited efficacy has been observed in patients with metastatic mismatch-repair proficient
27 (pMMR) colorectal cancer⁵. Here we report clinical results and in-depth analysis of patients with early-
28 stage pMMR colon cancer from the phase II NICHE study (ClinicalTrials.gov: NCT03026140). A total of
29 31 patients received neoadjuvant treatment of nivolumab plus ipilimumab followed by surgery. The
30 response rate was 26% and included six patients with a major pathological response ($\leq 10\%$ residual
31 viable tumour). One patient with an ongoing clinical complete response did not undergo surgery.
32 Circulating tumour DNA (ctDNA) was positive in 26/31 patients at baseline, and clearance was
33 observed in 5/6 responders prior to surgery, while 19/20 non-responders remained ctDNA+.
34 Responses were observed despite a low tumour mutational burden in all tumours, while chromosomal
35 genomic instability scores were significantly higher in responders compared to non-responders.
36 Furthermore, responding tumours had significantly higher baseline expression of proliferation
37 signatures and TCF1, and imaging mass cytometry revealed a higher percentage of Ki-67⁺ cancer and
38 Ki-67⁺ CD8⁺ T cells in responders compared to non-responders. These results provide a comprehensive
39 analysis of response to neoadjuvant ICB in early-stage pMMR colon cancers and identify potential
40 biomarkers for patient selection.

41

42 **Main**

43 Colorectal cancers (CRC) can be divided into two biologically distinct subtypes based on the status of
44 the DNA mismatch-repair (MMR) system: MMR proficient (pMMR) and MMR deficient (dMMR)
45 tumours. While immune checkpoint blockade (ICB) has become standard of care in patients with
46 metastatic dMMR tumours^{1,6}, metastatic pMMR tumours remain largely unresponsive to ICB⁵. This
47 disparity has, at least in part, been attributed to the substantially lower tumour mutational burden
48 (TMB) seen in pMMR tumours.

49

50 In recent years, neoadjuvant ICB has shown high pathological response rates that were associated
51 with improved survival in various solid tumour types^{2-4,7,8}. Notably, in patients with non-metastatic
52 dMMR CRC, neoadjuvant ICB induced remarkably high response rates without disease recurrences⁹⁻
53 ¹³. Recent studies also suggest that neoadjuvant ICB induces responses in a subgroup of patients with
54 non-metastatic pMMR CRC¹⁴⁻¹⁶. Underlying mechanisms likely contributing to this high efficacy in
55 earlier disease stages include a higher abundance of tumour-infiltrating immune cells, improved T
56 cell function and a lower level of local and systemic immune suppression¹⁷⁻²¹.

57
58 Considering the lack of efficacy of ICB in patients with metastatic pMMR CRC, and considering that
59 pMMR tumours constitute 85% of non-metastatic colon cancers²², strategies aimed at the
60 development of effective immunotherapy regimens for patients with non-metastatic pMMR CRC are
61 of high interest. Preclinical data showed that the inhibition of prostaglandin E2 synthesis, a product
62 of the cyclooxygenase-2 (COX-2) pathway, suppresses tumour-promoting inflammation and may
63 enhance immunotherapy response²³.

64 Given these data, we sought to explore the effects of neoadjuvant nivolumab plus ipilimumab, with
65 or without selective COX-2 inhibition using celecoxib, in patients with early-stage pMMR colon
66 adenocarcinoma. Here we report clinical outcomes as well as in-depth translational analyses from
67 patients treated in the pMMR cohort of the phase II NICHE platform trial (NCT03026140).

68

69 **Patient and treatment characteristics**

70 From June 29th 2017 until July 26th 2021, 37 patients were screened for eligibility, of whom 33 were
71 randomized and started treatment with either nivolumab and ipilimumab alone ($n = 17$) or combined
72 with celecoxib ($n = 16$). The relatively slow accrual rate for this cohort, despite the high incidence of
73 pMMR colon cancers, is likely attributable to the generally assumed unresponsiveness of pMMR
74 colon cancers to immunotherapy, combined with the COVID-19 pandemic. The median age was 62
75 years (range 44-77) and 45% of patients were female. Among 33 patients, 18 patients (55%) had
76 lymph node positive disease as assessed on baseline computed tomography (CT) scan (Table 1). Two
77 patients, one from each treatment group, who retrospectively did not meet inclusion criteria, were
78 excluded from efficacy and translational analyses. One patient was found to have a mixed
79 adenocarcinoma and neuroendocrine carcinoma (MiNEN) in the resection specimen and the other
80 had metastatic disease at preoperative imaging which was retrospectively visible on baseline
81 imaging. Both patients had completed two cycles of ICB according to protocol and were included in
82 the safety analyses (Extended Data Fig. 1).

83

84 Treatment with short-course neoadjuvant ICB was generally well tolerated (Extended Data Table 1)
85 and extensive safety data have been previously reported^{9,24}. Both cycles of ICB were administered in
86 32/33 patients (97%). Celecoxib was discontinued in 3/16 patients randomized to that arm (19%)
87 after 15, 21, and 24 days due to toxicity that was deemed at least possibly related to this treatment,
88 including dyspepsia, dyspnoea and rash. Surgery was performed in 32/33 patients (97%) with a
89 median interval of 4.6 weeks (range 3.7-6.0) between the first cycle of immunotherapy and
90 resection, all without delays and with tumour-free margins. The remaining patient had a delay in
91 surgery due to grade 3 myositis and required long-term immunosuppressive treatment before
92 symptoms resolved. During this time, the patient underwent three-monthly endoscopies and CT-
93 scans, and by the time surgery could be performed safely there was evidence of an ongoing clinical
94 complete response and the patient waived surgery. The patient is under active surveillance without
95 signs for local or distant recurrence, with a current follow-up of 42 months after treatment (Fig. 1e).
96

97 **Clinical outcomes and ctDNA**

98 Out of the 31 patients included in the efficacy analyses, 30 patients underwent surgery. Response to
99 treatment was observed in 8/31 patients (26%, 95% confidence interval (CI): 12-45%) (Fig. 1a), which
100 included one patient with a clinical complete response who did not undergo surgery. Among the 30
101 patients who underwent surgery, 7 patients (23%) had a pathological response, defined as 50% or
102 less residual viable tumour (RV). Six of these 7 patients (6/30; 20%) had a major pathological
103 response (MPR, defined as 10% or less RV), of which three (10%) were pathological complete
104 responses (pCR), defined as no RV in both the primary tumour and lymph nodes (See Extended Data
105 Table 2 for responses in individual patients, including AJCC stage and RV). Importantly, responses
106 were observed across stages as assessed at baseline, with 4 out of 8 (50%) responders having stage 3,
107 2 (25%) stage 2 and 2 (25%) stage 1 tumours, indicating that clinical high-risk pMMR tumours are also
108 amenable to response to neoadjuvant ICB. Response rates were comparable in patients treated with
109 or without celecoxib (4/15; 27% and 4/16; 25%, respectively).

110 Eight patients had tumour positive lymph nodes in their resection specimen and seven of these
111 patients, all non-responders, received adjuvant chemotherapy. The remaining patient, a responder
112 with a pCR in the primary tumour and partial response in lymph nodes, declined adjuvant
113 chemotherapy after counselling. One patient received adjuvant chemotherapy based on baseline
114 clinical staging and local pathological staging of an ypT4b tumour macroscopically invading the
115 abdominal wall, while central histopathological assessment revealed an ypT3 tumour.

116
117 Circulating tumour DNA (ctDNA) was detected in 26/31 patients (84%) at baseline, including 6
118 responders and 20 non-responders. CtDNA concentrations were associated with baseline clinical
119 staging, with the highest concentrations observed in patients with stage 3 disease (Extended Data
120 Fig. 2a). Analysis of ctDNA dynamics in patients who were ctDNA-positive at baseline showed
121 clearance of ctDNA prior to surgery either after the first ($n = 3$) or second cycle ($n = 2$) in 5 out of 6
122 responders. One responder remained ctDNA+ after the first cycle and no pre-surgical data were
123 available to assess clearance after the second cycle. In contrast, 19/20 (95%) non-responders
124 remained ctDNA+ at both time points prior to surgery (Fig. 1b and Extended Data Fig. 2b). Two
125 patients, both non-responders, remained ctDNA+ at 3 weeks post-surgery.

126
127 With a median follow-up of 56 months (range 8-80 months), 25 out of 31 patients in the efficacy
128 analysis (81%) were alive and disease-free, while six patients (19%) experienced disease recurrence,
129 of which one patient died due to disease progression. Median overall survival (OS) and disease-free
130 survival (DFS) were not reached (Fig. 1c). Among all patients in the efficacy analysis, the 3-year DFS
131 was 93% (95% CI: 85-100%). The two patients excluded from the efficacy analysis both received
132 chemotherapy, and one patient also underwent local treatment for liver metastases. Both patients
133 were disease-free and alive at the time of data cut-off, with a follow-up of 61 and 69 months,
134 respectively.

135 Notably, all responders remained disease-free, while all 6 patients with disease recurrence were
136 pathological non-responders and all were still ctDNA+ prior to surgery (Fig. 1d). Of the 2 patients that
137 remained ctDNA+ post-surgery, one had disease recurrence while the other patient, who had
138 received adjuvant chemotherapy due to tumour-positive lymph nodes, remained disease-free.

139
140 **Response-associated genomic features**

141 Whole-exome sequencing (WES) was performed to characterise genomic features of pMMR tumours
142 and to identify potential biomarkers of response to ICB in an exploratory analysis. All patients had a
143 low TMB (range 0.8 to 8.8 mutations/Mb), and TMB was not significantly higher in responders
144 compared to non-responders (median 3.3 vs. 2.7 mutations/Mb, $P = 0.13$) (Fig. 2b). In addition to
145 mutational burden, tumour immunity may be affected by the landscape of chromosomal and copy
146 number alterations, which reflects the level of genomic instability. Interestingly, responders

147 presented significantly higher chromosomal genomic instability scores compared to non-responders
148 (median 0.83 vs. 0.40, $P = 0.028$) (Fig. 2c), which was furthermore associated with more frequent
149 whole-genome duplication events (75% vs. 43%) (Fig. 2d, Extended Data Fig. 3a). Using a weighted
150 genome instability index (wgII) cut-off of 0.2 as a surrogate metric for chromosomal instability
151 (CIN^+)^{25,26}, 23/31 (74%) tumours were labelled as CIN^+ . Notably, the median wgII score was higher in
152 responders, with 7 out of 8 tumours classified as CIN^+ (Extended Data Fig 3b).

153
154 Analysis of known CRC driver mutations revealed frequent mutations in *APC* (94%), *TP53* (65%) and
155 *KRAS* (58%) (Fig. 2a), all determined to have functional impact (Supplementary Table 1). All 20 *TP53*
156 mutations had OncoKB loss of function or ClinVar pathogenic annotations. Importantly, most
157 responders harboured mutations in *TP53* (7/8, 88%), which were detected at a lower frequency in
158 non-responders (13/23, 57%) (Fig. 2f). Correspondingly, *TP53*mt tumours had a numerically higher
159 but not statistically significant response rate compared to *TP53*wt tumours (7/20, 35% vs. 1/11, 9%,
160 respectively, $P = 0.20$, Extended Data Fig. 3c). These data are in line with the overall higher rate of
161 genomic instability and proportion of whole-genome duplications in responders, both frequently
162 observed in *TP53*mt tumours (Extended Data Fig. 3d,e)²⁷.

163
164 Among the 18 tumours with pathogenic *KRAS* mutations, *KRAS*^{G12} substitutions were most frequent
165 ($n = 14$, 78%) and included 6 *KRAS*^{G12D}, 5 *KRAS*^{G12V}, 2 *KRAS*^{G12S} and 1 *KRAS*^{G12C} substitutions. In four
166 patients, other *KRAS* mutations were observed and included *KRAS*^{G13R}, *KRAS*^{G60V}, *KRAS*^{A146T} and
167 *KRAS*^{K117N}. All 18 *KRAS* mutations were gain of function. When considering all *KRAS* mutations, a non-
168 significant trend towards increased responses was observed in patients with *KRAS*wt tumours (5/13,
169 38%) compared to those with *KRAS*mt tumours (3/18, 17%, $P = 0.23$). Interestingly, when specifically
170 considering *KRAS*^{G12}, a response was observed in 1/14 (7%) tumours with a *KRAS*^{G12} mutation, while
171 7/17 (41%, $P = 0.045$) *KRAS*^{G12}wt tumours responded (Fig. 2e). Altogether, these data suggest a
172 possible enrichment for response in *TP53*mt; *KRAS*^{G12}wt tumours (6/13; 46%) (Fig. 2f) as compared to
173 limited responses in *TP53*mt; *KRAS*^{G12}mt (1/7, 14%) and *TP53*wt; *KRAS*^{G12}mt (0/7, 0%) tumours.

174

175 **Baseline proliferation and response**

176 To characterise molecular features of the tumour microenvironment (TME), a comprehensive set of
177 gene expression signatures was investigated (Supplementary Table 2). Transcriptomic analysis of pre-
178 treatment samples showed that immune-related signatures, including those associated with IFN- γ , T
179 cell infiltration and activity, were not predictive of response (Fig. 3a). However, signatures related to
180 cell proliferation and cell cycle were enriched in responders, including hallmarks for G2M checkpoint
181 ($P = 0.004$), E2F ($P = 0.012$) and MYC targets ($P = 0.03$) as well as a proliferation signature ($P = 0.026$,
182 Fig. 3b). Of note, the most pronounced association with response was a signature of NK cell receptor
183 ligands ($P = 2 \times 10^{-4}$), which was in turn correlated with the proliferation signature ($P = 3.9 \times 10^{-5}$,
184 Extended Data Fig. 4a). In addition, expression of TCF1 (encoded by *TCF7*), a marker of naïve or stem-
185 like T cells with proliferative potential²⁸, was significantly higher in responders compared to non-
186 responders ($P = 0.0074$). Furthermore, an enrichment of the hallmark signature for DNA repair was
187 observed in responders ($P = 0.0087$), consistent with the increased genomic instability in these
188 tumours, as described above.

189

190 To explore TME features of untreated *TP53*mt versus *TP53*wt pMMR colon cancer, we analysed
191 transcriptomic and genomic data from the cancer genome atlas (TCGA) and atlas and compass of
192 immune-colon cancer-microbiome interactions (AC-ICAM)²⁹ cohorts (Extended Data Table 3). This
193 revealed higher expression of proliferation and cell cycle signatures in *TP53*mt tumours (Extended
194 Data Fig. 3f-h, 4b). Strikingly in our study, even within tumours harbouring *TP53* mutations, scores for
195 these signatures were still higher in responders versus non-responders, suggesting that proliferation
196 may be an independent predictive biomarker (Fig. 3c).

197
198 To further investigate the cellular origin of the proliferation signal, Ki-67⁺ immunodetection alongside
199 several cellular markers was performed by imaging mass cytometry (IMC). The majority of Ki-67⁺ cells
200 corresponded to cancer cells (Extended Data Fig. 4c) and, in line with the transcriptomic data, a
201 significantly higher percentage of Ki-67⁺ cancer cells was observed in responders compared to non-
202 responders ($P = 0.004$, Extended Data Fig. 4d). Although cancer cell proliferation was predominant,
203 the density of Ki-67⁺ CD8⁺ T cells was also significantly higher in responders compared to non-
204 responders ($P = 0.035$, Fig. 3d), an observation that is of particular relevance in view of the previously
205 described association between intratumoural T cell proliferation and tumour reactivity³⁰. Notably,
206 the previously reported finding of a higher baseline CD8⁺PD-1⁺ infiltration in responders²⁴ was
207 numerically but not statistically significantly higher in this complete cohort and thus previous results
208 could not be confirmed ($P = 0.17$, Fig. 3e). However, a higher percentage of CD103 positivity, a tissue-
209 residency marker consistent with tumour-reactive populations in CD8⁺ T cells³¹, was associated with
210 response, albeit not significant ($P = 0.07$, Fig. 3f). To further dissect T cell phenotypes, single-cell RNA
211 sequencing (scRNASeq) and TCR sequencing was performed on CD45⁺ cells in pre-treatment biopsies,
212 which were available for 3 responders and 10 non-responders. The majority of immune cells
213 represented T/NK cells (Extended Data Fig. 4e, f). Most TCR clones corresponded to singletons, with
214 CD8⁺ T cells generally showing significantly greater clonal expansion than CD4⁺ T cells ($P = 7.2 \times 10^{-5}$).
215 When comparing CD4⁺ and CD8⁺ TCR clonality between responders and non-responders, no
216 significant differences were observed ($P = 0.37$ and $P = 0.47$, Fig. 3g, Extended Data Fig. 4g). CD8⁺ T
217 cells displayed distinct transcriptomic states that translated to 8 clusters, annotated with a
218 comprehensive combination of markers and scRNASeq signatures (Fig. 3h, Supplementary Table 2).
219 Importantly, CD8 cluster c4, a tissue-resident population with highest CD103 expression (encoded by
220 *ITGAE*), displayed transcriptomic markers of dysfunctional/exhausted cells, such as *ENTDP1*, *PDCD1*,
221 *TOX* and *CXCL13*, as well as checkpoints such as *TIGIT*, *LAG3* and *CTLA-4* (Fig. 3i, Extended Data Fig.
222 4i). Cluster c4 shared many of these transcriptomic features with the small proliferating cluster c7.
223 Furthermore, most TCR clones from the proliferating compartment were shared with those observed
224 in the c4 exhausted cell compartment (Fig. 3g,i). Consistently, both CD8⁺CD103⁺ and CD8⁺Ki-67⁺ T
225 cells, as well as clusters c4 and c7, were enriched for tumour-reactivity signatures (Extended Data Fig.
226 4h,j,k). While differences in CD8⁺ T cell cluster proportions were subtle between responders and non-
227 responders profiled with scRNASeq, these data support observations in IMC, by showing enrichment
228 for tumour-reactive cell states in the CD103⁺ and Ki-67⁺ CD8⁺ T cell pools that were associated with
229 response in the larger IMC data set.
230
231 To investigate innate-like immune cells relevant for the colon mucosa, $\gamma\delta$ T cells and innate lymphoid
232 cell (ILC) counts were retrieved from the IMC data. $\gamma\delta$ T cells were present at low frequencies and did
233 not differ at baseline ($P = 0.94$, Extended Data Fig. 4l). A trend towards higher density of ILC was
234 observed in responders ($P = 0.12$), with higher CD103 and Ki-67 expression in these cells, similar to
235 observations in CD8⁺ T cells (Extended Data Fig. 4m,n). Although representing the smallest TCR
236 negative cluster, ILC could be identified in scRNASeq data (Extended Data Fig. 4o) as ILC3, positive for
237 transcription factor ROR γ t (encoded by *Rorc*). Furthermore, the cluster had detectable expression of
238 MHC-II, indicating an ability for antigen presentation.
239
240 **Immune activation regardless of response**
241 A paired transcriptomic analysis of matched pre- and post-treatment samples was conducted to
242 understand TME dynamics after ICB. This revealed clear immune mobilisation in the majority of
243 patients, as evidenced by differentially upregulated genes of interest that are associated with anti-
244 cancer immunity and cytotoxicity such as *CXCL13* ($P = 5.1 \times 10^{-5}$), *CD8* ($P = 1.4 \times 10^{-5}$) and *IFN- γ*
245 signatures ($P = 9.2 \times 10^{-6}$, Fig. 4a-c and Extended Data Fig. 5a,b). Importantly, this immune activation
246 was observed in both pathological responders as well as non-responders, and the expression of
247 immune-related signatures increased with comparable magnitudes in both groups (Fig. 4d).

248 Despite the similar immune mobilisation upon ICB, the dynamics of metabolic and stromal signatures
249 differed between responders and non-responders. Specifically, mean scores for fatty acid
250 metabolism and mTOR signalling increased in non-responders after treatment ($P = 0.0067$ and $P =$
251 0.048), indicative of metabolic reprogramming, while these signatures decreased in responders ($P =$
252 0.55 and $P = 0.016$) (Fig. 4d). In addition, a significant decrease in the matrix remodelling signature
253 was detected in responders ($P = 0.016$), potentially reflecting tumour cell clearance, whereas this
254 signal remained relatively stable in non-responders ($P = 0.8$). When comparing post-treatment
255 expression in responders versus non-responders, matrix remodelling ($P = 0.001$) and metabolic
256 signatures such as OxPhos ($P = 0.0022$) and glycolysis ($P = 0.0054$) were higher in non-responders
257 (Fig. 4e), while TCF1 expression was higher in responders ($P = 0.023$).

258 Treatment with celecoxib was aimed at reducing prostaglandin E2 production²³ and promoting anti-
259 tumour immunity, yet when comparing patients treated with versus without celecoxib,
260 immunomodulatory effects of celecoxib were not observed post-treatment (Fig. 4f and Extended
261 Data Fig. 5c). Also, when considering patients with high baseline COX-2 expression, no differences in
262 post-treatment immunomodulation were observed in patients who were treated with or without
263 celecoxib (Extended Data Fig. 5d,e).

264 To evaluate interactions of stromal features and immune infiltration with response, the TME of each
265 sample was classified into four distinct subtypes, i.e., depleted, fibrotic, inflamed, or inflamed-
266 fibrotic, based on previously described signatures³², and tumours were additionally classified using
267 the consensus molecular subtypes (CMS)³³ (Fig. 5a).

268 At baseline, there was evidence for two main TME subtypes, i.e., immune-depleted and inflamed-
269 fibrotic (Fig. 5b). Non-responding tumours were more often of the inflamed-fibrotic subtype (14/23,
270 61%) compared to responding tumours (2/8, 25%) (Fig. 5c). Non-responders were more often of the
271 CMS2 (11/23, 48%) and CMS4 (6/23, 26%) subtypes (Extended Data Fig. 6a), and each accounted for
272 6 of the 14 inflamed-fibrotic non-responding tumours. Inflamed-fibrotic tumours exhibited
273 significantly higher expression of signatures related to fibroblast and T cell TGF- β signalling ($P = 1.1 \times$
274 10^{-4} and $P = 9.1 \times 10^{-5}$, Fig. 5d,e), and this was in turn positively associated with signatures for cancer-
275 associated fibroblasts (CAFs) (Fig. 5f), immune infiltration (Fig. 5g) and matrix remodelling (Extended
276 Data Fig. 6b). Furthermore, IMC analysis of pre-treatment biopsies revealed high TGF- β counts in a
277 subgroup of non-responders ($P = 0.37$, Fig. 5h), with high levels of TGF- β in both cancer cells and
278 CAFs, as well as extracellular matrix deposits (Extended Data Fig. 6c,d). Based on these findings, IMC
279 markers were compared across CAF and myeloid populations to further profile these cell subsets.
280 While responders did not display an enrichment for distinct CAFs (Extended Data Fig. 7a,c,d), a trend
281 for higher density of monocytes and macrophages positive for CD163 ($P = 0.063$) and HLA-DR ($P =$
282 0.064) was observed in responders (Extended Data Fig. 7b,e,f).

283 To further dissect differences within non-responders and the effects of ICB according to TME
284 subtype, TME dynamics were investigated by comparing pre- and post-treatment samples. Inflamed-
285 fibrotic non-responding tumours still displayed enrichment of immune signatures post-treatment,
286 accompanied by an increase in mTOR signalling and fatty acid metabolism (Extended Data Fig. 6e,f).
287 Meanwhile, non-responders that were not inflamed-fibrotic at baseline showed stronger immune
288 activation after ICB, along with increases in stromal signatures (Extended Data Fig. 6e,g). Altogether,
289 these results suggest that TGF- β and stromal features correlate with expression of immune
290 signatures in an important proportion of non-responders and may represent immune suppressive
291 mechanisms hampering response to ICB.

292

293 **Discussion**

294 In this study, we show that neoadjuvant nivolumab plus ipilimumab exhibits promising anti-tumour
295 activity in patients with pMMR colon cancer, a tumour type previously considered refractory to
296 immunotherapy, with a response rate of 26% after only 4 weeks of treatment.

297

300 The current standard of care for patients with localised pMMR colon cancers consists of surgery,
301 followed by adjuvant chemotherapy in case of stage 3 disease, which may also be considered for stage
302 2 disease with high-risk factors, including pT4 disease³⁴. Adjuvant chemotherapy regimens, including
303 fluorouracil with or without oxaliplatin, have been shown to improve disease-free and overall survival.
304 However, no advancements have been made since the introduction of oxaliplatin in 2004 to increase
305 cure in this patient population³⁵. While acknowledging the limitations of cross-trial comparisons and
306 our small sample size, the pathological response rate of 26% following neoadjuvant immunotherapy
307 in the current study is numerically similar to the 21-23% response rate to neoadjuvant chemotherapy
308 in pMMR tumours in the OPTICAL and FOxTROT studies^{36,37}. While there is an ongoing interest in the
309 potential of celecoxib either in combination with immunotherapy, or as an addition to adjuvant
310 chemotherapy³⁸, the addition of celecoxib did not affect response rates or induce substantial
311 immunomodulation in our study.

312
313 Neoadjuvant treatment regimens are increasingly being used in patients with colon cancer, and data
314 from the FOxTROT study suggests a strong correlation between pathological response to neoadjuvant
315 chemotherapy and lower risk of recurrence³⁶. Over the last years, a growing number of studies has
316 started to explore neoadjuvant immunotherapy in patients with both pMMR and dMMR colon
317 cancer^{11,12,14,16,39}. For neoadjuvant immunotherapy, the association between response and improved
318 recurrence-free survival appears to be stronger compared to targeted therapies, as observed in
319 melanoma^{7,8}. In addition, support for a highly favourable survival in colon cancer patients with a
320 pathological response to neoadjuvant ICB is provided by the NICHE-2 study, in which 98% of patients
321 with locally advanced dMMR colon cancer had a pathological response to neoadjuvant
322 immunotherapy, and none of these patients had recurrent disease at a median follow up of 3 years^{9,10}.
323 In the current study, a similar relationship between pathological response and a high DFS can be
324 postulated, albeit with smaller numbers, with none of the eight responders experiencing disease
325 recurrence compared to 6/23 non-responders having recurrence of disease at a median FU of 48
326 months. It should be noted that 48% of patients in this efficacy analysis had tumours that were
327 classified as stage 1 or 2 at baseline, which have been linked to lower 5-year recurrence rates of around
328 5% and 12%⁴⁰, respectively. However, responses in our study were not limited to patients with stage 1
329 or 2 disease and were also observed in patients with stage 3 disease with a recurrence risk that has
330 previously been described at approximately 33%⁴⁰. An important limitation of neoadjuvant treatment
331 for colon cancer remains the limited ability to accurately predict lymph node metastases on CT-scans,
332 which may lead to overstaging and potential overtreatment when focusing on lymph node staging^{41,42},
333 but we do note that in this study clinical staging was associated with the detection of ctDNA at baseline.
334 Importantly, we also show that pre-surgical clearance of ctDNA is strongly correlated with pathological
335 response after neoadjuvant immunotherapy, as evidenced by ctDNA clearance in responders, while all
336 but one non-responder remained ctDNA+. These data are in line with results from NICHE-2 in locally
337 advanced dMMR tumours showing clearance of ctDNA in the majority of patients with an MPR or pCR
338 following neoadjuvant nivolumab plus ipilimumab¹⁰. Together, these results may provide new avenues
339 for adaptive neoadjuvant studies based on ctDNA.

340
341 Translational analyses of colon tumours and the surrounding TME both before and after neoadjuvant
342 ICB are of great interest to identify biomarkers of response to immunotherapy or chemotherapy,
343 thereby aiding future selection of patients most likely to benefit from either of these therapies.
344 Importantly, the neoadjuvant administration of immunotherapy in this study provides the window of

345 opportunity for a unique in-depth analysis of the colon cancer TME of responders versus non-
346 responders. The lack of response in metastatic pMMR colon cancers has been largely attributed to
347 their low TMB and lack of immune infiltration. Here, we demonstrate that deep pathological responses
348 can be induced by ICB in pMMR colon cancer despite a low TMB in all tumours. Furthermore,
349 established biomarkers predictive of response to immunotherapy, such as IFN- γ ^{43,44} and CD8⁺ T cell
350 infiltration⁴⁵, were not different between responders and non-responders at baseline, suggesting that
351 in colon cancer different mechanisms of immune evasion may dominate. In an exploratory analysis,
352 we observed hints of an enrichment for response in tumours with *TP53* mutations, with a higher
353 probability of response in those harbouring a *TP53* mutation without a *KRAS*^{G12} mutation. If validated
354 in larger studies, these data may enable selection of patients based on standard of care genomic
355 assessments of colorectal cancers. Consistent with an elevated response rate in tumours with *TP53*
356 mutations, responding tumours also displayed an enrichment of whole-genome duplications, which
357 has recently been linked to higher ICB responsiveness in other cancer types²⁷.
358 In addition, proliferation and cell cycle gene signatures, as well as Ki67⁺ tumour and CD8⁺ T cells, were
359 found to be associated with response to ICB. While higher baseline proliferation has been described in
360 responders to ICB in other cancer types^{44,46}, there have been no previous data directly connecting the
361 triad of *TP53* mutational status, proliferation signatures and ICB response. Of note, both proliferation
362 and whole-genome duplications can promote states of cell stress and marked chromosomal
363 instability^{25,27,47}, altered expression of antigens, and activation of mechanisms for elimination of
364 aneuploid cells^{48,49}. This may in part explain responses observed in tumours with high levels of genomic
365 instability in our study.

366
367 Altogether, these data provide early evidence for a possible role for ICB to enable immune targeting
368 of genetically unstable *TP53*mt tumours. Of note, while genomic instability may potentiate ICB
369 efficacy by exposing immune vulnerabilities, it may also lead to evolution of resistance mechanisms in
370 tumour cells^{48,50}. Gaining a better understanding of the intricate interactions between genomic
371 instability, immunogenicity and immune evasion in the context of ICB will be of importance to further
372 improve the treatment of pMMR CRC.

373 In line with the association of proliferation signatures and response, using IMC and scRNAseq we
374 detected a higher infiltration of Ki-67⁺ and CD103⁺ CD8⁺ T cells with features of
375 dysfunctional/exhausted tumour-reactive cells in responders. These cells represented a relatively
376 small proportion of the total T cell pool, and showed expression of *ITGAE* (CD103), *CXCL13*, *ENTDP1*,
377 *PDCD1*, and other checkpoint molecules consistent with prior antigen exposure and tumour reactivity.
378 These results are in line with reports of chronically stimulated tissue-resident CD8⁺ populations that
379 retain proliferative capacity and are thought to be involved in tumour control^{30,31}, and which have been
380 associated with better prognosis and tumour-reactivity in pMMR CRC^{51,52}.

381 When comparing pre- and post-treatment expression data, we found that ICB was able to induce
382 substantial immune mobilisation in both responding and non-responding tumours. These results
383 suggest that lack of overall immune activation may not form the predominant mechanism underlying
384 ICB resistance in non-metastatic pMMR colon cancer. The importance of non-immune TME
385 components in response to ICB is suggested by our observation that stromal inflamed-fibrotic TME
386 subtypes were associated with lack of response, while the magnitude of immune infiltration by itself
387 was not. Compared to other subtypes, inflamed-fibrotic tumours exhibited higher signalling of TGF- β ,
388 a potent negative regulator of cancer immunity that has been associated with immune-exclusion and
389 poor prognosis. Based on these results and previous data showing an association between TGF- β and

390 non-response in urothelial and gynaecological malignancies^{53,54}, it may be of interest to explore the
391 role of TGF- β in response to ICB in patients with pMMR colon cancer in future trials^{46,55-58}.

392

393 While a subset of patients with non-metastatic pMMR colon cancer is cured with standard of care
394 adjuvant chemotherapy, depending on stage, between 20-50% of patients, develop disease recurrence
395 despite this treatment⁵⁹. Within the NICHE platform study, we provide the first data demonstrating
396 deep pathological responses following a short treatment with neoadjuvant ICB in 26% of patients with
397 pMMR colon cancer^{9,24}. Based on our data, we envision prospective studies that stratify patients based
398 on *TP53* and *KRAS* status to validate the results from the current study. Exploratory studies of
399 treatments targeting KRAS and tumour stroma, including TGF- β , may in addition provide avenues for
400 the subgroup of non-responders to ICB.

401 In conclusion, our data indicate that a substantial proportion of patients with localised pMMR colon
402 cancer may benefit from neoadjuvant anti-PD1 plus anti-CTLA4. These promising clinical and
403 translational findings warrant validation in larger cohorts of selected patient populations.

- 404 **References**
- 405 1 André, T. *et al.* Pembrolizumab in Microsatellite-Instability-High Advanced Colorectal Cancer. *N Engl J Med* **383**, 2207-2218, doi:10.1056/NEJMoa2017699 (2020).
- 406
- 407 2 Blank, C. U. *et al.* Neoadjuvant versus adjuvant ipilimumab plus nivolumab in macroscopic stage III melanoma. *Nat Med* **24**, 1655-1661, doi:10.1038/s41591-018-0198-0 (2018).
- 408
- 409 3 Forde, P. M. *et al.* Neoadjuvant PD-1 Blockade in Resectable Lung Cancer. *N Engl J Med* **378**, 1976-1986, doi:10.1056/NEJMoa1716078 (2018).
- 410
- 411 4 Powles, T. *et al.* Clinical efficacy and biomarker analysis of neoadjuvant atezolizumab in operable urothelial carcinoma in the ABACUS trial. *Nat Med*, doi:10.1038/s41591-019-0628-7 (2019).
- 412
- 413
- 414 5 Le, D. T. *et al.* Mismatch repair deficiency predicts response of solid tumors to PD-1 blockade. *Science* **357**, 409-413, doi:10.1126/science.aan6733 (2017).
- 415
- 416 6 Overman, M. J. *et al.* Durable Clinical Benefit With Nivolumab Plus Ipilimumab in DNA Mismatch Repair-Deficient/Microsatellite Instability-High Metastatic Colorectal Cancer. *J Clin Oncol* **36**, 773-779, doi:10.1200/jco.2017.76.9901 (2018).
- 417
- 418
- 419 7 Menzies, A. M. *et al.* Pathological response and survival with neoadjuvant therapy in melanoma: a pooled analysis from the International Neoadjuvant Melanoma Consortium (INMC). *Nat Med* **27**, 301-309, doi:10.1038/s41591-020-01188-3 (2021).
- 420
- 421
- 422 8 Versluis, J. M. *et al.* Survival update of neoadjuvant ipilimumab plus nivolumab in macroscopic stage III melanoma in the OpACIN and OpACIN-neo trials. *Ann Oncol* **34**, 420-430, doi:10.1016/j.annonc.2023.01.004 (2023).
- 423
- 424
- 425 9 Chalabi, M. *et al.* Neoadjuvant Immunotherapy in Locally Advanced Mismatch Repair-Deficient Colon Cancer. *N Engl J Med* **390**, 1949-1958, doi:10.1056/NEJMoa2400634 (2024).
- 426
- 427 10 Chalabi, M. *et al.* LBA24 Neoadjuvant immunotherapy in locally advanced MMR-deficient colon cancer: 3-year disease-free survival from NICHE-2. *Ann Oncol* **35**, S1217-S1218, doi:10.1016/j.annonc.2024.08.2263 (2024).
- 428
- 429
- 430 11 Shiu, K.-K. *et al.* NEOPRISM-CRC: Neoadjuvant pembrolizumab stratified to tumour mutation burden for high risk stage 2 or stage 3 deficient-MMR/MSI-high colorectal cancer. *J Clin Oncol* **42**, LBA3504-LBA3504, doi:10.1200/JCO.2024.42.17_suppl.LBA3504 (2024).
- 431
- 432
- 433 12 Cerck, A. *et al.* Nonoperative Management of Mismatch Repair-Deficient Tumors. *N Engl J Med* **392**, 2297-2308, doi:10.1056/NEJMoa2404512 (2025).
- 434
- 435 13 Hu, H. *et al.* Neoadjuvant PD-1 blockade with toripalimab, with or without celecoxib, in mismatch repair-deficient or microsatellite instability-high, locally advanced, colorectal cancer (PICC): a single-centre, parallel-group, non-comparative, randomised, phase 2 trial. *The Lancet. Gastroenterology & hepatology* **7**, 38-48, doi:10.1016/s2468-1253(21)00348-4 (2022).
- 436
- 437
- 438
- 439
- 440 14 Hissong, E. *et al.* Neoadjuvant botensilimab (BOT) plus balstilimab (BAL) in resectable mismatch repair proficient (pMMR) and deficient (dMMR) colorectal cancer (CRC): NEST clinical trial update. *J Clin Oncol* **43**, 207-207, doi:10.1200/JCO.2025.43.4_suppl.207 (2025).
- 441
- 442
- 443 15 Avallone, A. *et al.* 491P Neoadjuvant nivolumab in early stage colorectal cancer. *Ann Oncol* **31**, S449, doi:10.1016/j.annonc.2020.08.602 (2020).
- 444
- 445 16 Ghelardi, F. *et al.* Preoperative botensilimab (BOT) with or without balstilimab (BAL) for patients with resectable locally advanced pMMR or dMMR colon cancer: Results from the UNICORN trial by GONO. *ASCO GI* **43**, 158-158, doi:10.1200/JCO.2025.43.4_suppl.158 (2025).
- 446
- 447
- 448 17 Pagès, F. *et al.* Effector memory T cells, early metastasis, and survival in colorectal cancer. *N Engl J Med* **353**, 2654-2666, doi:10.1056/NEJMoa051424 (2005).
- 449
- 450 18 Versluis, J. M., Long, G. V. & Blank, C. U. Learning from clinical trials of neoadjuvant checkpoint blockade. *Nat Med* **26**, 475-484 (2020).
- 451
- 452 19 Mlecnik, B. *et al.* The tumor microenvironment and Immunoscore are critical determinants of dissemination to distant metastasis. *Sci Transl Med* **8**, 327ra326, doi:10.1126/scitranslmed.aad6352 (2016).
- 453
- 454

- 455 20 Mlecnik, B. *et al.* Integrative Analyses of Colorectal Cancer Show Immunoscore Is a Stronger
456 Predictor of Patient Survival Than Microsatellite Instability. *Immunity* **44**, 698-711,
457 doi:10.1016/j.jimmuni.2016.02.025 (2016).
- 458 21 Ben-Baruch, A. Inflammation-associated immune suppression in cancer: the roles played by
459 cytokines, chemokines and additional mediators. *Seminars in cancer biology* **16**, 38-52,
460 doi:10.1016/j.semancer.2005.07.006 (2006).
- 461 22 Eikenboom, E. L. *et al.* Universal Immunohistochemistry for Lynch Syndrome: A Systematic
462 Review and Meta-analysis of 58,580 Colorectal Carcinomas. *Clin Gastroenterol Hepatol* **20**,
463 e496-e507, doi:10.1016/j.cgh.2021.04.021 (2022).
- 464 23 Zelenay, S. *et al.* Cyclooxygenase-Dependent Tumor Growth through Evasion of Immunity.
465 *Cell* **162**, 1257-1270, doi:10.1016/j.cell.2015.08.015 (2015).
- 466 24 Chalabi, M. *et al.* Neoadjuvant immunotherapy leads to pathological responses in MMR-
467 proficient and MMR-deficient early-stage colon cancers. *Nat Med* **26**, 566-576,
468 doi:10.1038/s41591-020-0805-8 (2020).
- 469 25 Burrell, R. A. *et al.* Replication stress links structural and numerical cancer chromosomal
470 instability. *Nature* **494**, 492-496, doi:10.1038/nature11935 (2013).
- 471 26 Papaccio, F. *et al.* Decoding chromosomal instability insights in CRC by integrating omics and
472 patient-derived organoids. *Journal of experimental & clinical cancer research : CR* **44**, 77,
473 doi:10.1186/s13046-025-03308-8 (2025).
- 474 27 Quinton, R. J. *et al.* Whole-genome doubling confers unique genetic vulnerabilities on
475 tumour cells. *Nature* **590**, 492-497, doi:10.1038/s41586-020-03133-3 (2021).
- 476 28 Escobar, G., Mangani, D. & Anderson, A. C. T cell factor 1: A master regulator of the T cell
477 response in disease. *Science immunology* **5**, doi:10.1126/sciimmunol.abb9726 (2020).
- 478 29 Roelands, J. *et al.* An integrated tumor, immune and microbiome atlas of colon cancer. *Nat
479 Med* **29**, 1273-1286, doi:10.1038/s41591-023-02324-5 (2023).
- 480 30 Li, H. *et al.* Dysfunctional CD8 T Cells Form a Proliferative, Dynamically Regulated
481 Compartment within Human Melanoma. *Cell* **176**, 775-789.e718,
482 doi:10.1016/j.cell.2018.11.043 (2019).
- 483 31 Duhen, T. *et al.* Co-expression of CD39 and CD103 identifies tumor-reactive CD8 T cells in
484 human solid tumors. *Nat Commun* **9**, 2724, doi:10.1038/s41467-018-05072-0 (2018).
- 485 32 Bagaev, A. *et al.* Conserved pan-cancer microenvironment subtypes predict response to
486 immunotherapy. *Cancer Cell* **39**, 845-865.e847, doi:10.1016/j.ccr.2021.04.014 (2021).
- 487 33 Guinney, J. *et al.* The consensus molecular subtypes of colorectal cancer. *Nat Med* **21**, 1350-
488 1356, doi:10.1038/nm.3967 (2015).
- 489 34 Argilés, G. *et al.* Localised colon cancer: ESMO Clinical Practice Guidelines for diagnosis,
490 treatment and follow-up. *Ann Oncol* **31**, 1291-1305, doi:10.1016/j.annonc.2020.06.022
491 (2020).
- 492 35 André, T. *et al.* Oxaliplatin, fluorouracil, and leucovorin as adjuvant treatment for colon
493 cancer. *N Engl J Med* **350**, 2343-2351, doi:10.1056/NEJMoa032709 (2004).
- 494 36 Morton, D. *et al.* Preoperative Chemotherapy for Operable Colon Cancer: Mature Results of
495 an International Randomized Controlled Trial. *J Clin Oncol* **41**, 1541-1552,
496 doi:10.1200/jco.22.00046 (2023).
- 497 37 Hu, H. *et al.* Neoadjuvant Chemotherapy With Oxaliplatin and Fluoropyrimidine Versus
498 Upfront Surgery for Locally Advanced Colon Cancer: The Randomized, Phase III OPTICAL Trial.
499 *J Clin Oncol* **42**, 2978-2988, doi:10.1200/jco.23.01889 (2024).
- 500 38 Nowak, J. A. *et al.* Prognostic and predictive role of circulating tumor DNA (ctDNA) in stage III
501 colon cancer treated with celecoxib: Findings from CALGB (Alliance)/SWOG 80702. *J Clin
502 Oncol* (2025).
- 503 39 Starling, N. *et al.* AZUR-2, a phase III, open-label, randomized study of perioperative
504 dostarlimab monotherapy vs standard of care in previously untreated patients with T4N0 or
505 stage III dMMR/MSI-H resectable colon cancer. *JCO* **42**, TPS240-TPS240,
506 doi:10.1200/JCO.2024.42.3_suppl.TPS240 (2024).

- 507 40 Osterman, E. & Glimelius, B. Recurrence Risk After Up-to-Date Colon Cancer Staging, Surgery,
508 and Pathology: Analysis of the Entire Swedish Population. *Diseases of the colon and rectum*
509 **61**, 1016-1025, doi:10.1097/dcr.0000000000001158 (2018).
- 510 41 Shkurti, J. *et al.* Diagnostic accuracy of CT for local staging of colon cancer: A nationwide
511 study in the Netherlands. *Eur J Cancer* **193**, 113314, doi:10.1016/j.ejca.2023.113314 (2023).
- 512 42 Karoui, M. *et al.* Perioperative FOLFOX 4 Versus FOLFOX 4 Plus Cetuximab Versus Immediate
513 Surgery for High-Risk Stage II and III Colon Cancers: A Phase II Multicenter Randomized
514 Controlled Trial (PRODIGE 22). *Ann Surg* **271**, 637-645, doi:10.1097/sla.0000000000003454
515 (2020).
- 516 43 Ayers, M. *et al.* IFN- γ -related mRNA profile predicts clinical response to PD-1 blockade. *J Clin*
517 *Invest* **127**, 2930-2940, doi:10.1172/jci91190 (2017).
- 518 44 Rozeman, E. A. *et al.* Survival and biomarker analyses from the OpACIN-neo and OpACIN
519 neoadjuvant immunotherapy trials in stage III melanoma. *Nat Med* **27**, 256-263,
520 doi:10.1038/s41591-020-01211-7 (2021).
- 521 45 Tumeh, P. C. *et al.* PD-1 blockade induces responses by inhibiting adaptive immune
522 resistance. *Nature* **515**, 568-571, doi:10.1038/nature13954 (2014).
- 523 46 Mariathasan, S. *et al.* TGFbeta attenuates tumour response to PD-L1 blockade by
524 contributing to exclusion of T cells. *Nature* **554**, 544-548, doi:10.1038/nature25501 (2018).
- 525 47 Dewhurst, S. M. *et al.* Tolerance of whole-genome doubling propagates chromosomal
526 instability and accelerates cancer genome evolution. *Cancer Discov* **4**, 175-185,
527 doi:10.1158/2159-8290.cd-13-0285 (2014).
- 528 48 Kuang, X. & Li, J. Chromosome instability and aneuploidy as context-dependent activators or
529 inhibitors of antitumor immunity. *Front Immunol* **13**, 895961,
530 doi:10.3389/fimmu.2022.895961 (2022).
- 531 49 Santaguida, S. *et al.* Chromosome Mis-segregation Generates Cell-Cycle-Arrested Cells with
532 Complex Karyotypes that Are Eliminated by the Immune System. *Dev Cell* **41**, 638-651.e635,
533 doi:10.1016/j.devcel.2017.05.022 (2017).
- 534 50 Ben-David, U. & Amon, A. Context is everything: aneuploidy in cancer. *Nat Rev Genet* **21**, 44-
535 62, doi:10.1038/s41576-019-0171-x (2020).
- 536 51 Talhouni, S. *et al.* Activated tissue resident memory T-cells (CD8+CD103+CD39+) uniquely
537 predict survival in left sided "immune-hot" colorectal cancers. *Front Immunol* **14**, 1057292,
538 doi:10.3389/fimmu.2023.1057292 (2023).
- 539 52 van den Bulk, J. *et al.* CD103 and CD39 coexpression identifies neoantigen-specific cytotoxic T
540 cells in colorectal cancers with low mutation burden. *J Immunother Cancer* **11**,
541 doi:10.1136/jitc-2022-005887 (2023).
- 542 53 van Dijk, N. *et al.* Preoperative ipilimumab plus nivolumab in locoregionally advanced
543 urothelial cancer: the NABUCCO trial. *Nat Med* **26**, 1839-1844, doi:10.1038/s41591-020-
544 1085-z (2020).
- 545 54 Ni, Y. *et al.* High TGF- β signature predicts immunotherapy resistance in gynecologic cancer
546 patients treated with immune checkpoint inhibition. *NPJ Precis Oncol* **5**, 101,
547 doi:10.1038/s41698-021-00242-8 (2021).
- 548 55 Tauriello, D. V. F. *et al.* TGFbeta drives immune evasion in genetically reconstituted colon
549 cancer metastasis. *Nature* **554**, 538-543, doi:10.1038/nature25492 (2018).
- 550 56 Batlle, E. & Massagué, J. Transforming Growth Factor- β Signaling in Immunity and Cancer.
551 *Immunity* **50**, 924-940, doi:10.1016/j.jimmuni.2019.03.024 (2019).
- 552 57 Germann, M. *et al.* Neutrophils suppress tumor-infiltrating T cells in colon cancer via matrix
553 metalloproteinase-mediated activation of TGF β . *EMBO molecular medicine* **12**, e10681,
554 doi:10.15252/emmm.201910681 (2020).
- 555 58 Gulley, J. L. *et al.* Dual inhibition of TGF- β and PD-L1: a novel approach to cancer treatment.
556 *Mol Oncol* **16**, 2117-2134, doi:10.1002/1878-0261.13146 (2022).
- 557 59 Grothey, A. *et al.* Duration of Adjuvant Chemotherapy for Stage III Colon Cancer. *N Engl J*
558 *Med* **378**, 1177-1188, doi:10.1056/NEJMoa1713709 (2018).

559 **Tables & Figure Legends**

560

561 **Table 1. Baseline patient and tumour characteristics***

Characteristic	Overall (n = 33)
Age, median (range)	62 (44-77)
Sex (n (%))	
Female	15 (45%)
Male	18 (55%)
WHO performance status (n (%))	
0	31 (94%)
1	2 (6%)
Clinical disease stage (n (%))	
I	4 (12%)
II	11 (33%)
III	18 (55%)
Primary tumour location (n (%))	
Right	9 (27%)
Left	24 (73%)

* Baseline characteristics for all patients who received at least one cycle of study treatment.

562

563 **Fig. 1: Pathological responses and survival outcomes after short-course neoadjuvant ICB.**

564 **a**, Percentage of pathological regression shown per tumour. The dashed line demarcates PR at 50%
 565 regression and the black horizontal line depicts the demarcation for MPR at 90% regression. The upper
 566 bar marks the clinical stage at baseline (upper boxes), post-treatment pathological lymph node status
 567 (middle boxes) and whether patients received celecoxib (lower boxes). **b**, Association between
 568 pathological response and clearance of ctDNA pre-surgery, either after one or two cycles of treatment (n
 569 = 25). One responder who was ctDNA+ after cycle 1 and for whom no pre-surgical data were available,
 570 was excluded from this analysis. Significance was tested using a one-sided Fisher's exact test. **c**, Kaplan-
 571 Meier plot for overall survival in patients included in the efficacy analysis. **d**, Kaplan-Meier plot for
 572 disease-free survival for pathological responders (green) vs. non-responders (red) included in the
 573 efficacy analysis. **e**, Endoscopic images of the patient undergoing non-operative management with
 574 active surveillance, showing the tumour at baseline (upper panel) and a clinical complete response at 1
 575 year after treatment (lower panel).

576

577

578 **Fig. 2: Genomic features of pMMR responders and non-responders.**

579 **a**, Mutational landscape of pMMR tumours (n = 31), filtered for pathogenicity or likely functional impact
 580 (see Methods). Heatmap is coloured by the number of mutations detected in each gene and ordered by
 581 mutation frequency. Each column represents a patient, with baseline clinical staging, celecoxib
 582 treatment and response annotations presented above. **b,c**, Comparison of tumour mutational burden
 583 (TMB) (**b**) and ASCAT genomic instability scores (**c**) between responders (n = 8) and non-responders (n =
 584 23). Boxplots represent the median and interquartile range, whiskers extend from the hinge to the
 585 largest value within 1.5 x interquartile range from the hinge. Distributions were compared with a two-
 586 sided Wilcoxon rank-sum test. **d**, Proportion of tumours with whole-genome duplication in response
 587 groups. **e**, Frequency of KRAS mutations in responders (n = 8) and non-responders (n = 23). **f**,

588 Combination of *TP53* and *KRAS* mutational status and associations with response. *KRAS*^{G12}wt groups
589 include *KRAS*wt ($n = 13$) and other *KRAS* mutants ($n = 4$).
590
591

592 **Fig. 3: Baseline gene signatures, proliferation, and T cell populations in responders and non-**
593 **responders.**

594 **a**, Volcano plot comparing gene set expression for responders ($n = 8$) and non-responders ($n = 23$). Gene
595 sets are coloured by TME categories. The dashed horizontal line indicates $P = 0.05$, the dotted line FDR =
596 0.33, the dashed vertical line null effects. **b**, Proliferation ssGSEA scores between responders ($n = 8$) and
597 non-responders ($n = 23$). **c**, E2F targets, G2M checkpoint and proliferation signature in *TP53*mt
598 responders ($n = 7$) and non-responders ($n = 13$). **d**, Density of Ki-67⁺CD8⁺ in IMC samples for responders
599 ($n = 8$) and non-responders ($n = 22$). **e**, Density of CD8⁺PD-1⁺ T cells in immunohistochemistry for
600 responders ($n = 8$) and non-responders ($n = 21$). **f**, Percentage of CD103⁺ in CD8⁺ cells in IMC biopsies for
601 responders ($n = 8$) and non-responders ($n = 22$). **g**, Percentage of non-singleton scRNAseq-TCR
602 repertoires for all, CD8⁺ and CD4⁺ T cells in responders ($n = 3$) and non-responders ($n = 10$). Comparisons
603 include response groups and CD8⁺ vs. CD4⁺ for all patients ($n = 13$). **h**, UMAP of CD8⁺ T cell clusters ($n =$
604 4588). **i**, Dotplot of CD8⁺ T cell clusters and within-sample cluster distributions between responders ($n =$
605 3) and non-responders ($n = 9$), indicating log2 fold change between mean cluster proportions. One non-
606 responder was excluded due to low CD8⁺ T cells. Triangle: non-responder with a 0.71 proportion c3 CD8⁺
607 MAIT cells. Full cluster names: c0 activated memory, c1 naïve memory, c2 tissue-resident, c3 mucosal-
608 associated invariant, c4 exhausted, c5 early exhausted, c6 TNK effector, c7 proliferating. **b-f,g,i**, Boxplots
609 represent the median and interquartile range, whiskers extend from the hinge to the largest value
610 within 1.5 x interquartile range from the hinge. **a-f,g,i** Distributions were compared with two-sided
611 Wilcoxon rank-sum tests.
612
613

614 **Fig. 4: Immune mobilisation after ICB in responders and non-responders.**

615 **a-c**, Comparison of paired pre- and post-treatment expression for CD8⁺ T cells Danaher (**a**), Ayers
616 interferon- γ expanded (**b**) and *CXCL13* (**c**) in responders ($n = 8$) and non-responders ($n = 23$). Boxplots
617 represent the median and interquartile range, whiskers extend from the hinge to the largest value
618 within 1.5 x interquartile range from the hinge. Distributions were compared with a two-sided Wilcoxon
619 signed-rank test. **d**, Comparison of paired treatment effect sizes between response groups. Solid
620 diagonal line indicates a correlation of 1, dashed lines indicate null effects. Gene sets are coloured by
621 TME categories. **e**, Volcano plot comparing post-treatment expression of gene sets for responders ($n =$
622 8) and non-responders ($n = 23$). Gene sets are coloured by TME categories. The dashed vertical line
623 indicates null effects. **f**, Comparisons of post-treatment gene set expression between patients treated
624 with celecoxib ($n = 15$) or without ($n = 16$). Gene sets are coloured based on expectation of COX-2
625 inhibition/knockout from literature. **e-f**, Distributions were compared with two-sided Wilcoxon rank-
626 sum tests. Adjustment for multiple comparisons was performed to obtain the FDR. The dashed
627 horizontal line indicates $P = 0.05$ and the dotted line FDR = 0.33.
628
629

630 **Fig. 5: Association of TME subtypes and TGF- β signalling with response to ICB**

631 **a**, Heatmap of TME signature scores³². Values are Z-scored and coloured by discrete quantiles. Each
632 column represents a tumour sample ($n = 62$), with response, time point, baseline clinical staging,
633 consensus molecular subtypes (CMS)³³ and TME classifications annotated above. **b**, Proportion of TME

634 subtypes in pre-treatment samples for all tumours ($n = 31$), responders ($n = 8$) and non-responders ($n =$
635 23). **c**, Alluvial plots indicating TME classification between pre- and post-treatment samples for each
636 patient in response groups. **d,e**, Comparison of pre-treatment ssGSEA scores for fibroblast TGF- β
637 response signature (F TBRS) (**d**) and ssGSEA scores for T cell TGF- β response signature (T TBRS) (**e**) in
638 inflamed-fibrotic ($n = 16$) and non-inflamed fibrotic tumours ($n = 15$). Green triangles indicate
639 responders and red dots indicate non-responders. **f,g**, Correlation between pre-treatment ssGSEA scores
640 for cancer-associated fibroblasts and TGF- β hallmark signatures (**f**) and for cancer-associated fibroblasts
641 and TIL score signatures (**g**) for responders ($n = 8$) and non-responders ($n = 23$). Dots are coloured by
642 TME classification. The grey area indicates the 95% confidence interval of the blue regression line.
643 Pearson's r values and fits are shown. **h**, Comparison of total TGF- β counts per area in pre-treatment
644 IMC samples for responders ($n = 8$) and non-responders ($n = 22$). The dashed line indicates the median
645 TGF- β density. Boxplots represent the median and interquartile range, whiskers extend from the hinge
646 to the largest value within 1.5 x interquartile range from the hinge. Distributions were compared with a
647 two-sided Wilcoxon rank-sum test.
648

649 **Methods**

650

651 **Patients**

652 Eligible patients were 18 years or older and had previously untreated, pMMR, clinical stage I, II or III
653 colon adenocarcinoma that was considered resectable and showed no signs of distant metastases. All
654 patients had a World Health Organization (WHO) performance status of 0 or 1 and adequate
655 hematologic and end-organ function. MMR status was determined by immunohistochemical staining for
656 the MMR proteins MLH1, PMS2, MSH2 and MSH6 and proficiency was defined as normal expression of
657 all four proteins. Key exclusion criteria included signs of obstruction or perforation, prior
658 immunotherapy, active autoimmune disease requiring systemic immunosuppressive treatment, and
659 active concurrent cancer.

660

661 **Study design**

662 The NICHE study (Clinicaltrials.gov: NCT03026140) is an investigator-initiated, open-label study that was
663 conducted at the Netherlands Cancer Institute (NKI). All patients received a single dose of ipilimumab 1
664 mg/kg on day 1 and two doses of nivolumab 3 mg/kg on day 1 and 15, and patients were randomized to
665 additionally receive celecoxib 200 mg daily from day 1 until the day prior to surgical resection. Surgery
666 was scheduled in one of the participating centres with a predefined maximum of 6 weeks after study
667 enrolment. All treatment cycles were administered prior to surgery and no standard adjuvant study
668 treatment was given. According to national guidelines, adjuvant chemotherapy was offered to patients
669 who had tumour-positive lymph nodes or ypT4 status in the post-treatment resection specimen.

670

671 **Endpoints and statistics**

672 The primary objectives were safety and feasibility. The primary objective of safety was evaluated by the
673 occurrence of (serious) adverse events ((S)AEs) and the objective of feasibility was assessed by
674 treatment-related complications leading to surgical delay past the planned 6 weeks after inclusion in the
675 study as well as by adherence to the study protocol. All patients who received at least once cycle of the
676 study treatment were monitored for serious adverse events (SAEs) and adverse events (AEs) until 100
677 days after study drug administration and all AEs were graded according to the National Cancer Institute
678 Common Terminology Criteria for Adverse Events v4.03⁶⁰. Secondary and translational endpoints
679 included disease free survival (DFS), overall survival (OS) and efficacy as measured by histopathologic
680 treatment response as well as assessment of putative biomarkers of response and exploration of
681 treatment-induced changes in the tumour microenvironment based on genomics, transcriptomics,
682 immunohistochemistry and imaging mass cytometry.

683 Initial data regarding safety, efficacy and translational endpoints obtained from the first 17 patients
684 enrolled in the pMMR cohort and treated with nivolumab plus ipilimumab with or without celecoxib
685 have previously been published²⁴. The current report includes data on both the previously published
686 patients ($n = 17$) and the patients included thereafter ($n = 16$).

687

688 All patients underwent tumour staging at baseline by computed tomography (CT) of the chest and
689 abdomen performed within 28 days prior to start of treatment. Colonoscopy to obtain representative
690 pre-treatment biopsies from tumour and normal colon tissue was performed within 7 days before the
691 first treatment cycle and post-treatment tissue was obtained by surgical resection. All obtained tissue
692 samples were either directly frozen or fixed in formalin and paraffin embedded.

693
694 Clinical data were collected using TENALEA Clinical Trial Data Management system. Baseline
695 characteristics are presented for the intention-to-treat population, defined as all patients enrolled in the
696 study. Categorical variables are summarised as absolute numbers and percentages and continuous
697 variables with medians and (interquartile) ranges. For binary outcomes, exact two-sided 95% confidence
698 intervals were calculated using the Clopper-Pearson method. Time-to-event endpoints include DFS and
699 OS. DFS was defined as the time from surgery to recurrence or disease-related death; patients alive at
700 the last follow-up date who did not experience progression/recurrence were censored. OS was defined
701 as the time between the date of enrolment and death due to any cause; data for patients who are not
702 reported as having died are censored at the date when last known to be alive. The Kaplan-Meier method
703 was used to analyse time-to-event endpoints. A log-rank test was used to compare DFS and OS curves
704 between responders and non-responders; for comparison of the OS curves, landmark analysis was
705 performed with a landmark at the date of surgery. Median follow-up time from enrolment was
706 calculated using the reverse Kaplan-Meier method. All reported *P* values are two-sided unless otherwise
707 specified, and a *P* value of <0.05 was considered statistically significant. Analyses were performed using
708 R v4.3.0⁶¹ using R-studio build 561 with packages: arsenal v3.6.3, survival v3.6-4 and survminer v.0.4.9,
709 except for statistical analyses related to RNA sequencing, whole-exome sequencing,
710 immunohistochemistry and imaging mass cytometry data which were conducted using R v4.2.3 using R-
711 studio build 513 with the packages: tidyverse v2.0. ggplot2 v3.4.2, ggpahr v0.6.0 and pheatmap v1.0.12.
712 Exploratory comparisons of signature expression scores and genomic features were performed between
713 responders and non-responders using two-sided Wilcoxon rank-sum tests. Comparisons between pre-
714 and post-treatment samples were tested using Wilcoxon signed-rank tests. Multiple hypothesis testing
715 correction was performed with the method from Benjamini & Hochberg. Nominal *P* values are provided
716 and values corresponding to 0.33 FDR are indicated. Each patient represented a unit of analysis.
717

718 **Study oversight**

719 The study protocol was approved by the institutional review board of the NKI (sponsor) and by the
720 individual ethics boards of participating centres: OLVG and Spaarne Gasthuis. The study was conducted
721 in accordance with the International Conference on Harmonization Guideline for Good Clinical Practice
722 and the principles of the Declaration of Helsinki. Written informed consent for participation in the study
723 was obtained from all patients.

724

725 **Pathology assessments and immunohistochemistry**

726 Formalin-fixed, paraffin-embedded (FFPE) blocks were obtained from pre-treatment biopsies and from
727 post-treatment surgical specimens. Baseline tumour biopsies were used to assess MMR status by
728 immunohistochemistry for MLH1, PMS2, MSH2 and MSH6 performed on a BenchMark Ultra autostainer
729 (Ventana Medical Systems) following manufacturer's instructions. Briefly, 3 µm sections were cut from
730 FFPE blocks which were heated for 28 minutes at 75 °C and deparaffinised using EZ Prep solution
731 (Ventana Medical Systems). Heat-induced antigen retrieval was performed for 32 minutes at 95 °C using
732 Cell Conditioning Solution 1 (CC1, Ventana Medical Systems). The antibodies used for staining were
733 MLH1, Ready-to-use, M1 (6472966001, Roche); PMS2, 1:40 dilution, clone EP51 (M3647, Agilent
734 Technologies); MSH2, Ready-to-Use, G219-1129 (5269270001, Roche); MSH6, 1:50 dilution, EP49 (AC-
735 0047, Abcam). The OptiView DAB Detection Kit was used to visualize bound antibody and slides were
736 counterstained with Haematoxylin and Bluing Reagent (Ventana Medical Systems). Individual stains for

737 each protein were regarded as positive in case of clear nuclear staining in tumour cells with a positive
738 internal control. Tumours with positive staining for all four proteins were considered MMR proficient.
739

740 Post-treatment surgical specimens were subjected to histopathological examination using the entire
741 tumour bed and all resected lymph nodes. Slides were counterstained with haematoxylin and eosin
742 (H&E) to assess percentage of residual viable tumour (RVT).⁶² Pathological response was defined as
743 ≤50% RVT (consistent with AJCC/CAP TRG 0-2⁶³), including partial response with 11-50% RVT (AJCC/CAP
744 TRG 2), major pathological response (MPR) with ≤10% RVT (AJCC/CAP TRG 0-1), and pathological
745 complete response (pCR) with absence of RVT in both the tumour bed and lymph nodes (AJCC/CAP TRG
746 0).⁶² Post-treatment specimens were also staged according to the AJCC 8th TNM classification.⁶⁴ All
747 specimens were centrally reviewed by an experienced gastrointestinal pathologist.
748

749 FFPE sections obtained from pre-treatment tumour biopsies were evaluated by immunohistochemistry
750 for PD-1 and CD8 using a Discovery Ultra autostainer (Ventana Medical Systems). Briefly, FFPE blocks
751 were used to cut 3 µm sections, which were heated for 28 minutes at 75 °C and deparaffinised using EZ
752 Prep solution (Ventana Medical Systems). Heat-induced antigen retrieval was performed for 32 minutes
753 at 95 °C using Cell Conditioning Solution 1 (CC1, Ventana Medical Systems). A double stain was
754 performed for PD-1 (yellow) followed by CD8 (purple). In the first sequence, PD-1 was detected using
755 clone NAT105 (ready-to-use, Roche Diagnostics, Ventana Medical Systems) for 32 minutes at 37 °C and bound
756 antibody was visualized using Anti-Mouse NP (Ventana Medical Systems) for 12 minutes at 37 °C,
757 followed by the Discovery Yellow detection kit (Ventana Medical Systems). In the second sequence, CD8
758 was detected using clone CD8/144B (1:200 dilution, Agilent/DAKO) at 32 minutes for 37 °C and bound
759 antibody was visualized using Anti-Mouse HQ (Ventana Medical Systems) for 12 minutes at 37 °C,
760 followed by the Discovery Purple Detection Kit (Ventana Medical Systems). Slides were counterstained
761 with Haematoxylin and Bluing Reagent (Ventana Medical Systems). All slides were scanned with the
762 Panoramic 1000 (3D HISTECH) at 0.25 µm per pixel. HALO image analysis software v4.0.5107.357 (Indica
763 Labs)⁶⁵ was used for quantification of positively stained cells within the tumour region that was
764 manually annotated by a gastrointestinal pathologist. The Indica Labs Multiplex IHC v3.0.3 analysis
765 algorithm was used for the analysis.
766

767 **Circulating tumour DNA analysis**

768 SignateraTM (Natera Inc.) circulating tumour (ctDNA) analysis was performed retrospectively on banked
769 specimens. Whole-exome sequencing was conducted on tumour tissue and on matched germline DNA
770 obtained from PBMCs. Following initial quality controls and sample concordance checks, somatic variant
771 calling was performed using Natera's proprietary bioinformatics pipeline⁶⁶, which allows filtering of
772 putative germline and clonal haematopoiesis mutations of unknown significance. Up to 16 somatic
773 single-nucleotide variants were selected, based on which PCR amplicons were designed and applied on
774 cell-free DNA (cfDNA) samples of all patients.
775

776 A median of 29.25 ng cfDNA was isolated from a median of 4.0 ml (range 1.7-7.4 ml) plasma obtained
777 from all patients at baseline, prior to cycle 2, pre-operative as well as 3 weeks and 3-6 months post-
778 operative. Plasma samples were considered to be ctDNA-positive when ≥2 out of 16 variants were
779 detected. The concentration of ctDNA in each sample was measured and reported as mean tumour
780 molecules per millilitre of plasma.

781
782 Categorical variables were compared using Fisher's exact test, carried out in R version 4.3.1 using
783 packages stats (v4.3.1) and mosaic (v.1.9.1).

784

785 **Imaging mass cytometry staining and analysis**

786 IMC was performed on pre-treatment biopsies using 4 µm thick FFPE tissue sections to detect 40 cellular
787 targets as described previously.⁶⁷ After deparaffinising and heat-mediated antigen retrieval in high pH
788 antigen retrieval solution (eBioscience, Thermo Fisher Scientific), sections were subjected to blocking
789 with Superblock solution (Thermo Fisher Scientific) to limit unspecific binding of antibodies. Next,
790 antibodies were incubated overnight at 4 °C with anti-CD4 and anti-TCR gamma delta (antibody details
791 are available in supplementary table 3) followed by a 5 hour room temperature incubation with the first
792 set of antibodies. After rigorous washing, the sections were incubated with the remaining antibodies
793 and incubated for 5 minutes with DNA intercalator Iridium (1.25 µM, Fluidigm) to stain the nuclei.
794 Finally, sections were washed with water, air-dried and stored at room temperature until measurement.

795

796 For each section, two or three 1 mm² regions of interest were ablated on the Hyperion mass cytometry
797 imaging system (Fluidigm). Data quality was visually inspected using the Fluidigm mcd viewer
798 (v1.0.560.6) and exported as multi-tiff files. Images were normalised by rescaling all images and markers
799 between 0 and 1 followed by a two-step denoising, where first a minimal signal threshold of 0.1 was set
800 followed by per marker percentile normalisation. Cell segmentation masks were generated from the
801 normalised images using CellProfiler (v4.2.1). First nuclei were defined using the DNA images to which
802 membranes were added using keratin, vimentin and CD45 images. Single cell marker expression FCS files
803 were generated by combining the normalised images with cell segmentation masks in ImaCytE⁶⁸ and
804 after dimensionality reduction, cells were clustered by mean-shift clustering in Cytosplore (v2.3.1).⁶⁹
805 Clusters were mapped back on the images and visually confirmed by comparison with raw images in
806 MCD viewer. Finally, cluster abundances per image were combined per sample and visualized as
807 cells/mm². Counts were averaged across regions of interest for each sample. Due to low abundance of
808 CD103 and Granzyme B, no distinct clusters were formed and thus their presence was determined by
809 counting the number of cells with a marker expression above 0.2 in each T cell cluster.

810

811 **Genomic and transcriptomic analysis**

812 Whole-exome sequencing was conducted on tumour DNA isolated from pre-treatment biopsies and
813 matched germline DNA from peripheral blood samples to assess the mutational landscape. RNA was
814 isolated from pre- and post-treatment tumour samples and was sequenced to evaluate expression of
815 various immune- and tumour-related gene signatures.

816

817 Fresh-frozen tumour samples obtained pre- and post-treatment were used for DNA and RNA isolation. A
818 cryostat was used to cut 10 µm sections intended for isolation and a consecutive 5 µm section used to
819 initially assess tumour percentage. This 5 µm section was H&E stained and a pathologist scored tumour
820 cell percentage and indicated the relevant tumour region. Samples were selected for isolation using a
821 tumour percentage of at least 30%, except for post-treatment samples from tumours with an MPR or
822 pCR. DNA and RNA were isolated simultaneously from 10 µm sections with the AllPrep DNA/RNA/miRNA
823 Universal isolation kit (Qiagen, 80224) by using the QIAcube, according to manufacturer's protocol. If
824 fresh-frozen material was unavailable or if tumour content was insufficient, FFPE sections were used
825 instead. A pathologist scored tumour percentage and indicated the most tumour-dense region for
826 isolation on an H&E stained slide. Depending on tumour size, 5-10 10 µm sections were cut and DNA and

827 RNA were isolated simultaneously with the AllPrep DNA/RNA FFPE isolation kit (Qiagen, #80234) using
828 the QIAcube, according to manufacturer's protocol. Normal germline DNA was obtained from 1 ml
829 peripheral blood and was extracted by using the QIAasympathy DNA Blood 1000 (DNA Midi kit, 96),
830 according to manufacturer's protocol.

831

832 **DNA sequencing and analysis**

833 The concentration of double stranded DNA was quantified in each sample using the Qubit® dsDNA HS
834 Assay Kit (Invitrogen, cat no Q32851). Covaris AFA technology was used to fragment a maximum amount
835 of 2 µg double stranded genomic DNA into fragment sizes of 200-300 bp. Sample purification was
836 carried out using Agencourt AMPure XP Reagent (Beckman Coulter, cat no A63881) in 2x reaction
837 volume settings according to manufacturer's instructions. Quantity and quality of fragmented DNA was
838 measured on a BioAnalyzer system using the DNA7500 assay kit (Agilent Technologies cat no. 5067-
839 1506). NGS library preparation for Illumina sequencing was conducted with the KAPA HTP Prep Kit
840 (KAPA Biosystems, KK8234) using xGen UDI-UMI Adapters of IDT 10bp (Integrated DNA Technologies). A
841 4-cycle PCR was performed to amplify libraries in order to obtain sufficient yield for exome enrichment.
842 Quantification of DNA libraries was done on a BioAnalyzer system using the DNA7500 assay kit. Exome
843 enrichment was conducted on library pools of 8 unique dual indexed libraries (500 ng each) using the
844 xGen™ Exome Hyb Panel v2 (IDT, cat no 10005152) and xGen™ Hybridization Capture Core Reagents
845 following manufacturer's instructions where hybridization time was adjusted to 20 hours and 10 cycles
846 of PCR were performed during post-capture PCR. All exome enriched library pools were quantified on a
847 BioAnalyzer system with the DNA7500 assay kit, pooled equimolar to a 10 nM final concentration,
848 followed by paired-end 100bp sequencing on either an Illumina HiSeq 2500 using V2 chemistry or an
849 Illumina Novaseq 6000 instrument using a NovaSeq 6000 S4 Reagent Kit v1.5 (Illumina, 20028313) and a
850 S2 Reagent kit v1.5 (Illumina, 20028315), according to manufacturer's protocol.

851

852 Whole-exome sequencing data were processed using Sarek v3.1.2.⁷⁰, a pipeline that follows GATK best
853 practices and is distributed by NF-core. Samples were aligned to GRCh38 using bwa v0.7.17, duplicates
854 were marked with MarkDuplicates (GATK pipeline v4.3) and base quality scores were recalibrated with
855 BaseRecalibrator (GATK pipeline v4.3). Germline and somatic indels and single nucleotide variants were
856 called with Strelka2 v2.9.10⁷¹, annotated with snpeff v5.1 and ensemblvep v106.1. Only variants with at
857 least 20X depth and 5% variant allele frequency were considered. Tumour mutational burden was
858 calculated as the number of non-synonymous and frameshift variants divided by the target BED
859 coverage size (39 Mb).

860 For assessing functional impact of mutations, variants were filtered based on the following criteria:
861 Mutations were considered if they had moderate or high impact by snpeff or consensual (likely)
862 pathogenic annotations in ClinVar⁷², while variants with only benign and likely benign annotations were
863 removed. Variants of either uncertain significance, conflicting evidence (e.g. pathogenic & benign) or no
864 ClinVar data available were considered if structural predictions were deleterious or damaging, with
865 either SIFT scores below 0.05 or PolyPhen-2 scores above 0.446. Mutated genes were only included on
866 heatmaps and considered functionally affected if they passed these filters. Furthermore, non-
867 synonymous mutations were converted with vcf2maf (v1.6.22) and annotated with OncoKB annotator
868 (v3.4.1) to obtain gain of function and loss of function OncoKB annotations⁷³. Copy number variation
869 calling, genome integrity scores and whole-genome duplication states were obtained with ASCAT v3.0⁷⁴.
870 ASCAT genome integrity scores measure the fraction of the copy-number profile deviating from a ploidy

871 of 2n or deviating from 4n for whole-genome duplicated tumours. Additionally, the weighted genome
872 integrity index^{25,26} was used as a surrogate for chromosomal instability with a cutoff of 0.2. This was
873 calculated as the percentage of ASCAT heterozygous sites deviating from the median baseline ploidy by
874 at least 0.6, averaged across the 22 autosomal chromosomes.

875

876 Bulk RNA sequencing and analysis

877 Quality and quantity of the total RNA was assessed on the 2100 Bioanalyzer instrument using an Agilent
878 RNA 6000 Nano chip (G2938-90034, Agilent Technologies) following manufacturer's instructions. The
879 region method analysis was used according to the manufacturer's manual (technical-note-470-2014-
880 001, Illumina, Inc.) to determine the percentage of RNA fragments with >200 nt fragment distribution
881 values (DV200).

882 Strand-specific libraries were generated using the TruSeq RNA Exome Library Prep Kit (Illumina, Inc.)
883 according to manufacturer's instructions (Illumina, Inc. no. 1000000039582v01), with the following
884 adaptation: samples that contained intact total RNA were subjected to the optional heat fragmentation
885 step (94°C for 8 minutes, 4 °C hold). For the initial 15 pre-treatment and 14 post-treatment samples, the
886 generated cDNA fragments were ligated to TruSeq RNA Single Indexes adapters (20020492/20020493,
887 Illumina, Inc.), and for the remaining samples IDT xGen UDI(10bp)-UMI(9bp) paired-end sequencing
888 adapters (Integrated DNA Technologies) were used. All cDNA fragments were amplified by 15 cycles of
889 PCR. The libraries were validated on a 2100 Bioanalyzer instrument following the manufacturer's
890 protocol of the Agilent DNA 7500 kit (G2938-90025, Agilent Technologies), followed by a 1-4 plex library
891 pooling containing up to 200ng of each sample. The pooled cDNA libraries were enriched for target
892 regions using the probe Coding Exome Oligos set (CEX, 45MB, Illumina, Inc.) and 10 cycles of PCR. The
893 libraries were analysed on a 2100 Bioanalyzer instrument following the manufacturer's protocol of the
894 Agilent DNA 7500 kit (G2938-90025, Agilent Technologies), then diluted to 10nM and pooled equimolar
895 into multiplex sequencing pools. Libraries of the initial 15 pre-treatment and 14 post-treatment samples
896 were sequenced with 65 base single reads on a HiSeq2500 using V4 chemistry (Illumina, Inc.) and
897 demultiplexed using bcl2fastq2. For the remaining samples, the libraries were sequenced with 54 cycles
898 for Read 1, 19 cycles for Read i7, 10 cycles for Read i5 and 54 cycles for Read 2 on a NovaSeq6000 using
899 a Reagent Kit v1.5 (100cycles) (Illumina, Inc.). Reads were demultiplexed using bclconvert and duplicates
900 were marked with rumidup (<https://github.com/NKI-GCF/rumidup>).

901

902 FASTQ files were aligned to GRCh38 using Hisat2 (v2.2.1), duplicate and strand-aware counted per gene
903 using gensem (<https://github.com/NKI-GCF/gensem>), and annotated with Ensembl GRCh38.107.
904 Differential expression was performed with DESeq2 v1.38.3 and enrichment analysis was performed
905 with enrichR v3.2 using genes with adjusted P values below 0.05. ssGSEA scores for curated signatures
906 (Supplementary Table 2) were calculated using the GSVA v1.46 package and gene sets consisting of
907 individual genes were compared using log2(RPM+1) values instead. Standardized mean differences
908 (Cohen's d) between response groups were calculated using the pooled standard deviation. Paired
909 treatment effect sizes were calculated as the mean difference between pairs divided by the standard
910 deviation. Pearson's r correlations were calculated using ggpubr (v0.6.0), fits and confidence intervals
911 from linear models were visualized with the geom_smooth (v3.4.2). TME subtypes were classified
912 manually based on Z-score heatmaps for Bagaev et al. signatures³². This was aided by using hierarchical
913 clustering and median signature scores, blinded to response groups. Consensus molecular subtype

914 (CMS) assignment was performed with the CMSclassifier random forest using the nearest CMS
915 classification (<https://github.com/Sage-Bionetworks/CMSclassifier>).
916

917 Single-cell RNA and TCR Sequencing

918 Fresh tumor biopsies were transferred onto ice in RPMI 1640 medium (Thermo Fisher Scientific)
919 supplemented with 2.5% fetal calf serum (FCS; Sigma-Aldrich) and 1% penicillin-streptomycin (pen/strep,
920 Roche). On ice, the samples were placed in petri dishes and dissected by hand into small fragments of
921 approximately 1–2 mm³ in size. These fragments were then suspended in 1 mL of freezing solution
922 consisting of FCS containing 10% dimethyl sulfoxide (DMSO; Sigma-Aldrich), and stored in liquid nitrogen
923 for long-term preservation.
924

925 At the day of sequencing, cryopreserved tumor fragments were rapidly thawed in a 37 °C water bath until
926 only a small ice crystal remained. To eliminate residual DMSO, the fragments were subsequently washed
927 three times using 7 mL wash medium [Dulbecco's Modified Eagle Medium (DMEM) supplemented with
928 10% FCS and 1% pen/strep] using 6-well plates and 45 µm cell-strainers. After this washing step, fragments
929 were left on ice until all samples were thawed. Subsequently, samples were digested in 2 mL digestion
930 medium consisting of RPMI 1640 supplemented with 1% pen/strep, Pulmozyme (12.6 µg/mL; Roche), and
931 collagenase type IV (1 mg/mL; Sigma-Aldrich) at 37 °C with continuous rotation for 45 minutes. Next,
932 samples were washed twice with cold phosphate-buffered saline (PBS) and transferred to 1.5 mL
933 Eppendorf tubes. Next, cells were resuspended in 25 µL of cold Cell Staining Buffer (BioLegend) containing
934 Human TruStain FcX (1:10 dilution; BioLegend) to block Fc receptors. For sample multiplexing, TotalSeq-C
935 anti-human hashtag antibodies (numbers 1–13; final concentration 1 µg/mL, BioLegend) were added and
936 incubated on ice for 30 minutes. Subsequently, 25 µL of Cell Staining Buffer containing anti-CD45-PerCP-
937 Cy5.5 (1:50; Invitrogen) and TotalSeq-C-conjugated antibodies targeting PD-1 (clone EH12-EH7, 1:1000),
938 CD39 (clone A1; 1:1000), CD137 (clone 4B4-1; 1:5000), CD8 (clone SK1, 1:5000), and CD4 (clone RPA-T4,
939 1:2500) were added. After another 30-minute incubation on ice, cells were washed three times using Cell
940 Staining Buffer. The cells were then resuspended in 500 µL MACS buffer (PBS with 0.5% bovine serum
941 albumin [BSA, Sigma] and 2 mM EDTA [Life Technologies]). To normalize cell input across samples, 5 µL
942 aliquots were taken and quantified using AccuCount Blank Particles (13.0–17.9 µm; Spherotech) on a BD
943 LSR Fortessa™ X-20 Cell Analyzer (BD Biosciences). Dead cells were excluded using propidium iodide (PI;
944 0.5 µg/mL; Sigma-Aldrich). Samples labeled with hashtag antibodies were then pooled, and live CD45+
945 immune cells were sorted using a FACSAria Fusion Flow Cytometer (BD Biosciences). Sorted cells were
946 collected in RPMI 1640 medium containing 10% human serum and 1% pen/strep, followed by sequential
947 washes with cold 1% BSA in PBS and 0.04% BSA in PBS. Finally, cells were resuspended in 0.04% BSA in
948 PBS at a target concentration of 800–1200 cells/µL, suitable for downstream single-cell RNA and T-cell
949 receptor sequencing using the 10x Genomics platform.
950

951 Between 10,000 and 20,000 sorted immune cells were loaded per lane on the 10X Chromium platform for
952 single-cell RNA sequencing. For each run, cells from 3 to 13 different biopsies were combined. Library
953 preparation for gene expression, TCR, and antibody-derived tags was performed following the
954 manufacturer's protocol using the Chromium Next GEM Single Cell V(D)J Reagent Kits (10X Genomics).
955 10X 5' single cell-sequencing was carried out on Illumina NovaSeq 6000 instrument, with target read
956 lengths of 26–28/58–130 bp in RNA and antibody libraries, and 26–28/92–130 bp for TCR libraries. The
957 sequencing depth was optimized to approximately 30,000 paired-end reads per cell for transcriptomic
958 data and 5,000 reads per cell for both antibody and TCR libraries.
959

960 **Single-cell RNA and TCR Sequencing data processing**
961 'Cell Ranger multi' version 7.1.0 was used to generate the gene and feature counts mapping to GRCh38-
962 2020-A as well as the VDJ assembly and clonotype assignment. The reference for the clonotype calling was
963 generated from the IMGT database (LIGM-DB 14.1), using the script provided by 10X Genomics. Single cell
964 data processing was done using R version 4.2.3, R-studio (Build 513) and the Seurat package v5.2.1⁷⁵. TCR
965 data was analyzed and integrated using scRepertoire v2.3.2⁷⁶.

966
967 Detected cells were filtered for quality control based on overall median values for genes, counts,
968 mitochondrial ("^MT-") and ribosomal protein RNA ("^RP[SL]") percentages. Cells passing quality control
969 had the number of genes and counts within the range of 1/5 up to 5 median values, below 5 medians of
970 mitochondrial percentage and above 1/3 of the median ribosomal protein RNA percentage. Additionally,
971 cells were filtered for a minimum of 200 genes, 1000 counts and a maximum of 30% mitochondrial RNA
972 percentage. The hashtag information in the feature counts was used to demultiplex filtered cells using
973 HTODemux, keeping singlet calls and excluding doublets. scRNAseq data was log-normalized using the
974 median library size as a scale factor, the top 2000 variable features were obtained, and the full dataset
975 was scaled. Principal component analysis was performed using 25 principal components, used for UMAP
976 representations. Cells were initially clustered using the FindNeighbours and FindClusters functions at a
977 resolution of 0.5. Broad cell type annotations were assigned per cluster using knowledge base markers
978 from Spectra⁷⁷ and Cellmarker⁷⁸, and also informed by automated scType labels. T and TNK populations,
979 corresponding to the set of non B-lineage lymphocytes, were separated and re-clustered at different
980 resolutions. All TCR-positive cells were assigned with CD4⁺ and CD8⁺ annotations based on normalized
981 antibody counts and CD8A/CD8B expression. TCR negative cells were annotated as CD8⁺ T cells if they
982 contained CD8A/CD8B counts or CD8 antibody expression and CD4⁺ T cells if they contained CD4
983 expression or antibody counts. CD8⁺ T cells, CD4⁺ T cells and other lymphocytes were separated, re-
984 clustered and annotated using knowledge base markers and signature scores, measured using
985 AddModuleScore_UCell (Supplementary Table 2).

986
987 **External Datasets**
988 Analysis of TCGA and AC-ICAM cohorts²⁹ was included for comparisons with external data of pMMR
989 colon cancer. Processed RNA and DNA sequencing data were downloaded using cBioportal.⁷⁹
990 Mutational status for the TCGA cohort was based on analysis from Grasso et al.⁸⁰ Samples with AJCC
991 pathological stage IV colon cancer or POLE mutations were excluded. For the TCGA cohort, genomic and
992 transcriptomic data were available for 287 and 276 patients, respectively. For the AC-ICAM cohort,
993 genomic and transcriptomic data were available for 173 patients with Stage I-III pMMR CC.

994
995 **Data availability**
996 DNA and RNA sequencing data for the NICHE study is deposited in the European Genome-phenome
997 Archive (EGA) under accession number EGAS5000000856. Data is under controlled access according to
998 consent provided by the patients whose samples are used and according to GDPR. Data will be made
999 available for academic use only upon reasonable request and within the confinements of the informed
1000 consent and the European Data Protection Regulation. Requests should include project descriptions
1001 describing the research goal, privacy, governance and intended use of data, and can be done through
1002 <https://ega.nki.nl/>, contacting repository@nki.nl. Requests will be reviewed by the institutional review
1003 board of the Netherlands Cancer Institute (NKI) and require signing of a data access agreement with the
1004 NKI after approval. The estimated time to response is 4-6 weeks with an expected total turnaround time
1005 of 4-6 months including drafting and approval of the data transfer agreement.

1006
1007 Clinical data from The Cancer Genome Atlas (TCGA) Research Network were obtained from the Clinical
1008 data resource Liu et al. 2018 (DOI: 10.1101/j.cell.2018.02.052). TCGA mutational status for CRC was
1009 obtained from analysis by Grasso et al. 2018, available as supplementary material (DOI: 10.1158/2159-
1010 8290.CD-17-1327). RNAseq data is openly available and was obtained from cBioPortal
1011 (<https://www.cbioportal.org>), with accession code coadread_tcga_pan_can_atlas_2018. Data for the
1012 AC-ICAM CC cohort is openly available and was downloaded from cBioPortal
1013 (<https://www.cbioportal.org>), with accession code coad_silu_2022.
1014
1015

- 1016 **Methods references**
- 1017
- 1018 60 Revised Common Terminology Criteria for Adverse Events (CTCAE) Version 4.03 (National Cancer
1019 Institute);
1020 https://ctep.cancer.gov/protocoldevelopment/electronic_applications/ctc.htm#ctc_40, 2010).
- 1021 61 R Core Team. R: A Language and Environment for Statistical Computing. R Foundation for
1022 Statistical Computing, Vienna, Austria (2023).
- 1023 62 Cottrell, T. R. *et al.* Pathologic features of response to neoadjuvant anti-PD-1 in resected non-
1024 small-cell lung carcinoma: a proposal for quantitative immune-related pathologic response
1025 criteria (irPRC). *Ann Oncol* **29**, 1853-1860, doi:10.1093/annonc/mdy218 (2018).
- 1026 63 Burgart, L. J., Chopp, W. V. & Jain, D. Protocol for the examination of resection specimens from
1027 patients with primary carcinoma of the colon and rectum.
1028 https://documents.cap.org/protocols/ColoRectal_4.2.0.2.REL_CAPCP.pdf. Published June 2022.
1029 Accessed April 9, 2025.
- 1030 64 Amin, M. B. *et al.* The Eighth Edition AJCC Cancer Staging Manual: Continuing to build a bridge
1031 from a population-based to a more "personalized" approach to cancer staging. *CA Cancer J Clin*
1032 **67**, 93-99, doi:10.3322/caac.21388 (2017).
- 1033 65 HALO Image Analysis Platform. Version 4.0.5107.357. Albuquerque, NM: Indica Labs, Inc.
1034 (2024).
- 1035 66 Reinert, T. *et al.* Analysis of Plasma Cell-Free DNA by Ultradeep Sequencing in Patients With
1036 Stages I to III Colorectal Cancer. *JAMA Oncol* **5**, 1124-1131, doi:10.1001/jamaoncol.2019.0528
1037 (2019).
- 1038 67 Ijsselsteijn, M. E., van der Breggen, R., Farina Sarasqueta, A., Koning, F. & de Miranda, N. A 40-
1039 Marker Panel for High Dimensional Characterization of Cancer Immune Microenvironments by
1040 Imaging Mass Cytometry. *Front Immunol* **10**, 2534, doi:10.3389/fimmu.2019.02534 (2019).
- 1041 68 Somarakis, A., Van Unen, V., Koning, F., Lelieveldt, B. & Höllt, T. ImaCytE: Visual Exploration of
1042 Cellular Micro-Environments for Imaging Mass Cytometry Data. *IEEE Trans Vis Comput Graph* **27**,
1043 98-110, doi:10.1109/tvcg.2019.2931299 (2021).
- 1044 69 Höllt, T. *et al.* in *Comput. Graph. Forum*. 171-180 (Wiley Online Library).
- 1045 70 Garcia, M. *et al.* Sarek: A portable workflow for whole-genome sequencing analysis of germline
1046 and somatic variants. *F1000Res* **9**, 63, doi:10.12688/f1000research.16665.2 (2020).
- 1047 71 Kim, S. *et al.* Strelka2: fast and accurate calling of germline and somatic variants. *Nat Methods*
1048 **15**, 591-594, doi:10.1038/s41592-018-0051-x (2018).
- 1049 72 Landrum, M. J. *et al.* ClinVar: public archive of relationships among sequence variation and
1050 human phenotype. *Nucleic Acids Res* **42**, D980-985, doi:10.1093/nar/gkt1113 (2014).
- 1051 73 Chakravarty, D. *et al.* OncoKB: A Precision Oncology Knowledge Base. *JCO Precis Oncol* **2017**,
1052 doi:10.1200/PO.17.00011 (2017).
- 1053 74 Ross, E. M., Haase, K., Van Loo, P. & Markowitz, F. Allele-specific multi-sample copy number
1054 segmentation in ASCAT. *Bioinformatics* **37**, 1909-1911, doi:10.1093/bioinformatics/btaa538
1055 (2021).
- 1056 75 Hao, Y. *et al.* Dictionary learning for integrative, multimodal and scalable single-cell analysis. *Nat
1057 Biotechnol* **42**, 293-304, doi:10.1038/s41587-023-01767-y (2024).
- 1058 76 Yang, Q., Safina, K. R. & Borcherding, N. scRepertoire 2: Enhanced and Efficient Toolkit for
1059 Single-Cell Immune Profiling. *bioRxiv*, 2024.2012.2031.630854, doi:10.1101/2024.12.31.630854
1060 (2024).
- 1061 77 Kunes, R. Z., Walle, T., Land, M., Navy, T. & Pe'er, D. Supervised discovery of interpretable gene
1062 programs from single-cell data. *Nat Biotechnol* **42**, 1084-1095, doi:10.1038/s41587-023-01940-3
1063 (2024).

- 1064 78 Hu, C. *et al.* CellMarker 2.0: an updated database of manually curated cell markers in
1065 human/mouse and web tools based on scRNA-seq data. *Nucleic Acids Res* **51**, D870-d876,
1066 doi:10.1093/nar/gkac947 (2023).
- 1067 79 Cerami, E. *et al.* The cBio cancer genomics portal: an open platform for exploring
1068 multidimensional cancer genomics data. *Cancer Discov* **2**, 401-404, doi:10.1158/2159-8290.cd-
1069 12-0095 (2012).
- 1070 80 Grasso, C. S. *et al.* Genetic Mechanisms of Immune Evasion in Colorectal Cancer. *Cancer Discov*
1071 **8**, 730-749, doi:10.1158/2159-8290.cd-17-1327 (2018).
- 1072

1073 **Acknowledgements**
1074 We thank all the patients and their families for participation in the present study. We thank the Core
1075 Facility of Molecular Pathology and Biobanking, in particular A. Broeks and S. Cornelissen for their
1076 support in processing of the samples; M. Nieuwland, C. van Steenis and W. Brugman and the Genomics
1077 Core Facility for their support with sequencing; the Research High Performance Computing Facility for
1078 data storage and computation infrastructure; L. Al-van Wijck and M. van den Belt from the scientific
1079 administration department for data management and support in trial conduct and management; T.
1080 Korse, M. Lucas and E. Platte for PBMC acquisition and processing; physicians, nurses and supportive
1081 personnel from the departments of gastrointestinal oncology, endoscopy, surgery and pathology and
1082 the in- and outpatient clinics for patient care. This study contains data from the TCGA Research
1083 Network. The present study was funded by the BMS International Immuno-Oncology Network and
1084 sponsored by the NKI. The funding source had no role in design and execution of the study, data analysis
1085 or writing of the manuscript.

1086 Analyses within this project were supported by a Fellowship from ESMO, supported by AstraZeneca.
1087 Any views, opinions, findings, conclusions, or recommendations expressed in this material are those
1088 solely of the authors and do not reflect those of ESMO or AstraZeneca. Research at the Netherlands
1089 Cancer Institute is supported by institutional grants of the Dutch Cancer Society (KWF) and of the Dutch
1090 Ministry of Health, Welfare and Sport.
1091

1092 **Author contributions**

1093 P.B.T. performed genomic and transcriptomic biomarker analyses under supervision of K.M, L.F.A.W and
1094 M.C. Y.L.V. analysed the clinical data and S.B. performed statistical analysis of clinical data. P.B.T. and
1095 Y.L.V. interpreted clinical and translational data and wrote the first draft of manuscript under
1096 supervision of M.C. J.G.v.d.B. performed histopathological scoring. M.E.I. and N.F.C.C.d.M. performed
1097 imaging mass cytometry and processed the data; analysis and interpretation of the data was performed
1098 together with P.B.T. and M.C. A.J. and A.T. analysed circulating tumour DNA and interpreted the data
1099 together with Y.L.V. and M.C. P.K. performed immune cell isolation from biopsies for single cell RNA and
1100 TCR sequencing. M.E.v.L. performed endoscopies and N.F.M.K. performed surgeries. E.E.V. was involved
1101 in study design. J.B.A.G.H., T.N.S. and M.C. made the experimental plan of investigation. M.C. was the
1102 principal investigator, designed the study, wrote the study protocol and coordinated trial procedures. All
1103 authors reviewed, edited and approved of the manuscript and vouch for the accuracy of the data
1104 reported and adherence to the study protocol.
1105

1106 **Competing interests**

1107 P.B.T., Y.L.V., J.G.v.d.B., S.B., N.F.M.K., M.E.I., K.M, M.E.v.L., N.F.C.C.d.M., P.K. declare no competing
1108 interests. A.J. and A.T. are employees of Natera, Inc. with stocks and/or stock options to own in the
1109 company. A.J. also owns stocks in lovance, Agenus and Versastem. J.B.A.G.H. is an advisor to Achilles
1110 Therapeutics, AstraZeneca, BioNTech, Bristol Myers Squibb, Curevac, Gadeta, Imcyse, Immunocore,
1111 lovance Therapeutics, Ipsen, Merck Serono, Merck Sharp & Dohme, Molecular Partners, Neogene
1112 Therapeutics, Novartis, Pfizer, PokeAcel, Roche, Sanofi, Sastra Cell Therapy, Third Rock Ventures and T-
1113 Knife and has received research grants unrelated to this study from Amgen, Asher Bio, BioNTech US,
1114 Bristol Myers Squibb, Merck Sharp & Dohme, Novartis and Sastra Cell Therapy. J.B.A.G.H. owns stock in
1115 Neogene Therapeutics. All grants were paid to the institution. E.E.V. reports research funding from
1116 Bristol Myers Squibb outside the current work. T.N.S. declares advisory roles for Allogene Therapeutics,
1117 Asher Bio, Merus, Neogene Therapeutics and Scenic Biotech, is stockholder in Allogene Therapeutics,

1118 Asher Therapeutics, Cell Control, Merus and Scenic Biotech, and is venture partner at Third Rock
1119 Ventures. L.F.A.W. received project funding from Bristol Myers Squibb outside the current work. M.C. is
1120 advisor to Bristol Myers Squibb, Kineta, Merck Sharp & Dohme, NOUSCOM and Roche/Genentech and
1121 has received research grants unrelated to this study from Bristol Myers Squibb, Agenus, Merck Sharp &
1122 Dohme and Roche/Genentech. All grants were paid to the institution.

1123

1124 **Additional information**

1125 Supplementary Information is available for this paper.

1126

1127 Correspondence should be addressed to the corresponding author (m.chalabi@nki.nl).

1128

1129

1130

1131 **Extended Data Legends**

1132

1133 Extended Data Fig. 1: Consort Flow Diagram.

1134 Flowchart of patients screened and randomized in the NICHE study.

1135

1136 Extended Data Fig. 2: Overview of ctDNA dynamics per patient.

1137 **a**, Baseline ctDNA concentration according to baseline clinical stage. The number and percentage of
1138 patients with positive ctDNA is indicated above each box. Boxplots represent the median and
1139 interquartile range, whiskers extend from the hinge to the largest value within 1.5 x interquartile range
1140 from the hinge. **b**, For each patient, the colored boxes indicate the post-treatment response (p/CCR:
1141 pathological/clinical complete response; MPR: major pathological response; PR: partial response; NR:
1142 non-response), baseline stage based on CT scan, whether adjuvant chemotherapy (CTx) was given along
1143 with the ctDNA status at baseline, prior to cycle 2, pre-operatively (pre-op), 3 weeks post-operatively
1144 (post-op 3W) and 3 to 6 months post-operatively (post-op 3-6M). Due to patient 86 not undergoing
1145 surgery, no sample was available for the pre-operative time point and samples obtained at 3 and 6
1146 months after the first cycle of immunotherapy were used as post-operative time points.

1147

1148 Extended Data Fig. 3: **Genomic and transcriptomic features of TP53mt tumours.**

1149 **a**, Comparison of ASCAT genomic instability scores between tumours with whole-genome duplication
1150 (WGD) ($n = 16$) and without ($n = 15$). **b**, Comparison of weighted genome integrity index between
1151 responders ($n = 8$) and non-responders ($n = 23$). Dashed horizontal line indicates a cut-off of 0.2 as a
1152 surrogate measure for chromosomal instability. Distributions were compared with a two-sided Wilcoxon
1153 rank-sum test. **c**, Response rates across *TP53*, *KRAS* and *KRAS^{G12}* mutated groups. Significance was tested
1154 using a two-sided Fisher's exact test. **d**, Comparison of genomic instability scores between *TP53mt* ($n =$
1155 20) and *TP53wt* tumours ($n = 11$). **e**, Proportion of tumours with whole-genome duplication in *TP53*
1156 groups. **f**, Volcano plot comparing expression of gene sets for *TP53mt* ($n = 20$) and *TP53wt* ($n = 11$)
1157 NICHE tumours pre-treatment. **g,h**, Volcano plot comparing expression of gene sets for *TP53mt* ($n = 165$)
1158 and *TP53wt* ($n = 111$) tumours in TCGA (**g**) and *TP53mt* ($n = 84$) and *TP53wt* ($n = 85$) tumours in AC-
1159 ICAM²⁹ (**h**). **a,b,d**, Boxplots represent the median and interquartile range, whiskers extend from the
1160 hinge to the largest value within 1.5 x interquartile range from the hinge. **f-h**, Gene sets are coloured
1161 based on distinct TME categories. Distributions were compared with two-sided Wilcoxon rank-sum tests.
1162 Adjustment for multiple comparisons was performed to obtain the FDR. The dashed horizontal line
1163 indicates a *P* value of 0.05 and the dotted line indicates an FDR of 0.33. The dashed vertical line indicates
1164 null effects.

1165
1166 **Extended Data Fig. 4. Pre-treatment associations of proliferation, NK receptor ligands, tumour-**
1167 **infiltrating lymphocyte phenotypes and response.**
1168 **a**, Correlation between NK receptor ligand and proliferation signature ($n = 31$). Data points are coloured
1169 and shaped by *TP53* and WGD status. The grey area indicates the 95% confidence interval of the blue
1170 regression line. Pearson's r values and fits are shown. **b**, Proliferation in *TP53mt* vs. *TP53wt* tumours in
1171 NICHE, AC-ICAM and TCGA cohorts. **c**, Percentage of total Ki-67⁺ cells across cell categories in IMC ($n =$
1172 30) **d**, Percentage of Ki-67⁺ cells in total, cancer and CD8⁺ cells in IMC for responders ($n = 8$) and non-
1173 responders ($n = 22$). **e**, scRNAseq UMAP ($n = 23947$), coloured by broad celltypes. **f**, Quantification of
1174 immune proportions for responders ($n = 3$) and non-responders ($n = 10$). The TNK cluster contains CD8⁺,
1175 NK and innate lymphoid cells. **g**, Total cells coloured by TCR detection, and proportion of TCR repertoires
1176 occupied by the top 20 clones, coloured by log2 frequencies for responders ($n = 3$) and non-responders
1177 ($n = 10$). **h**, Enrichment of scRNAseq tumour-reactivity signatures in CD103⁺ and Ki-67⁺ CD8⁺ T cells, **i-k**,
1178 Distribution of (**i**) CD8 Exhaustion, (**j**) Oliveira tumour specific and (**k**) NeoTCR8 signatures in CD8⁺ T cell
1179 clusters. **l-m** Comparison of $\gamma\delta$ T (**l**) and innate lymphoid cell (ILC) density (**m**) in IMC for responders ($n =$
1180 8) and non-responders ($n = 22$). **n**, Percentage of ILC positive for CD103 and Ki-67 in IMC for responders
1181 ($n = 7$) and non-responders ($n = 21$). **o**, Dotplot of ILC marker expression pooling all cells ($n = 80$). **b,d,l-n**
1182 Distributions were compared with two-sided Wilcoxon's rank sum tests. Boxplots represent the median
1183 and interquartile range, whiskers extend from the hinge to the largest value within 1.5 x interquartile
1184 range from the hinge.
1185

1186 **Extended Data Fig. 5: Differential expression of ICB and celecoxib treatment.**
1187 **a**, Paired differential gene expression of matched pre vs. post-treatment samples. Dashed horizontal line
1188 indicates an FDR of 0.05 ($n = 31$). **b**, Top 20 Reactome pathways enriched in differentially upregulated
1189 genes after treatment, based on log2(fold change) > 0 and FDR < 0.05. Bars are coloured by the fraction
1190 of the gene set that was differentially upregulated. **c**, Differential gene expression of post-treatment
1191 samples from patients treated with celecoxib ($n = 15$) or without ($n = 16$). Dashed horizontal line
1192 indicates an FDR of 0.05. Genes are coloured based on expectation of COX-2 inhibition/knockout from
1193 literature²³ **d**, Comparison of pre- and post-treatment expression of prostaglandin receptors and COX-2
1194 in patients randomized to receive celecoxib ($n = 15$) or not ($n = 16$). Boxplots represent the median and
1195 interquartile range, whiskers extend from the hinge to the largest value within 1.5 x interquartile range
1196 from the hinge. Distributions were compared with two-sided Wilcoxon's rank sum tests. Dashed line
1197 indicates the median pre-treatment COX-2 expression for high and low expression groups. **e**,
1198 Comparison of paired treatment effect sizes between patients with high baseline COX-2 expression
1199 treated with celecoxib ($n = 9$) or without ($n = 6$). Solid diagonal line indicates a correlation of 1, dashed
1200 lines indicate null effects. Gene sets are coloured based on distinct TME categories.
1201

1202 **Extended Data Fig. 6: Association of inflamed-fibrotic state with TGF- β signalling and matrix**
1203 **remodelling.**
1204 **a**, Frequency of consensus molecular subtypes (CMS) in pre-treatment samples for responders ($n = 8$)
1205 and non-responders ($n = 23$), coloured by TME subtypes. **b**, Comparison of pre-treatment ssGSEA scores
1206 for matrix remodelling in inflamed-fibrotic ($n = 16$) and non-inflamed fibrotic tumours ($n = 15$). The
1207 green triangles indicate responders and the red dots indicate non-responders. Distributions were
1208 compared with a two-sided Wilcoxon's rank sum test. Boxplots represent the median and interquartile
1209 range, whiskers extend from the hinge to the largest value within 1.5 x interquartile range from the
1210 hinge. **c,d** Illustrative IMC regions of interest for (c) a TGF- β high non-responder and (d) a TGF- β low

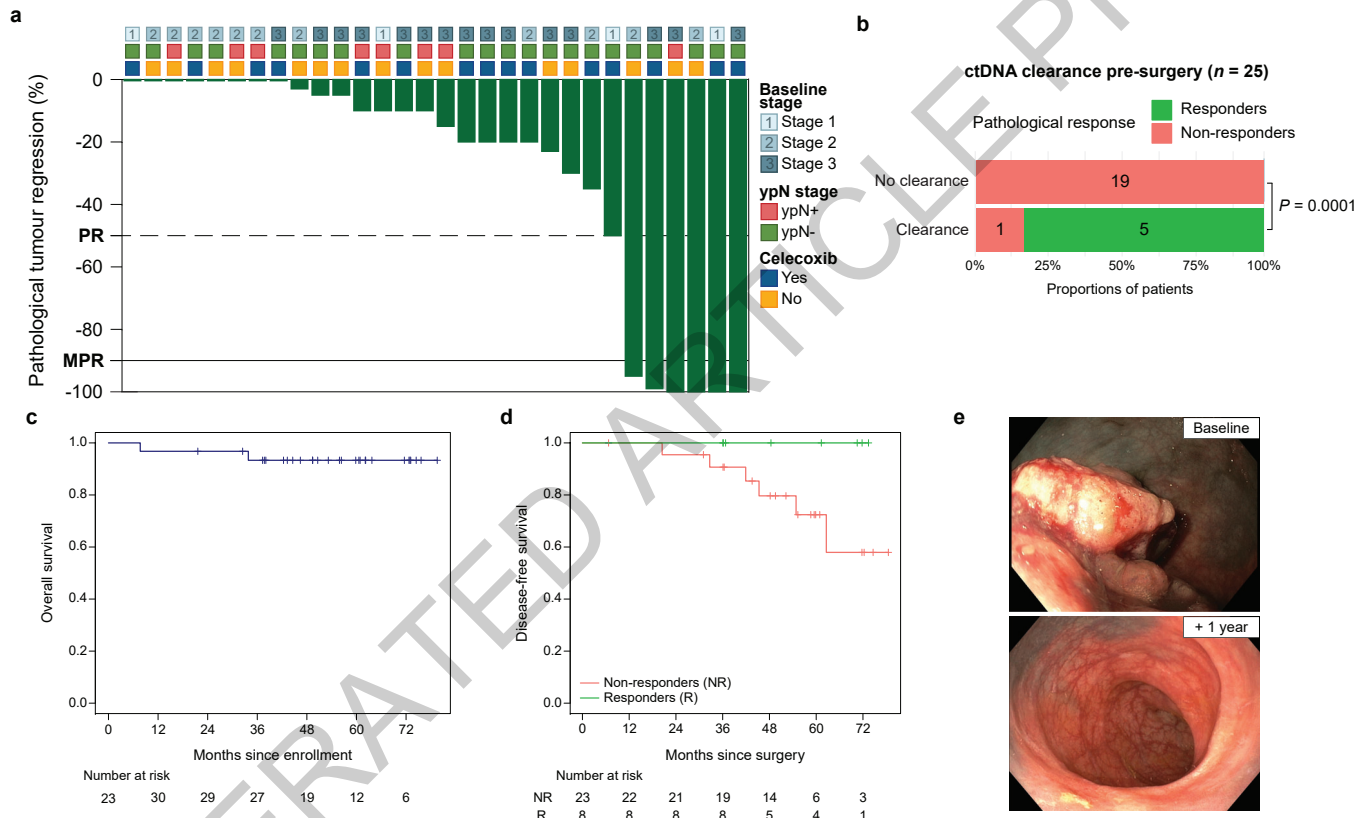
1211 responder sample. 2-3 regions of interest were obtained per patient biopsy in one independent
1212 experiment. Nuclei (DNA) are coloured in red, Keratin in blue and TGF- β in green. Scale bar: 100 μ M. **e-g**
1213 Comparison of paired treatment effect sizes between inflamed-fibrotic non-responders ($n = 14$) and non
1214 inflamed-fibrotic non-responders ($n = 9$) (**e**), responders ($n = 8$) and inflamed-fibrotic non-responders (n
1215 = 14) (**f**) and responders ($n = 8$) and non inflamed-fibrotic non-responders ($n = 9$) (**g**). Solid diagonal line
1216 indicates a correlation of 1, dashed lines indicate null effects. Gene sets are coloured based on distinct
1217 TME categories.
1218

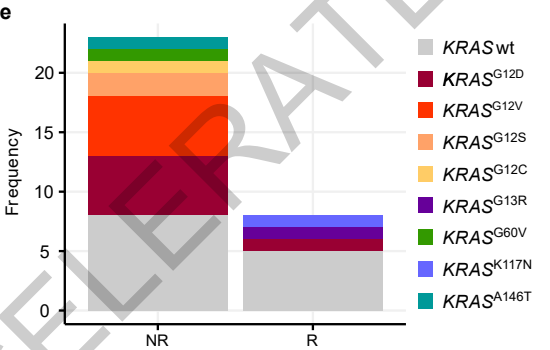
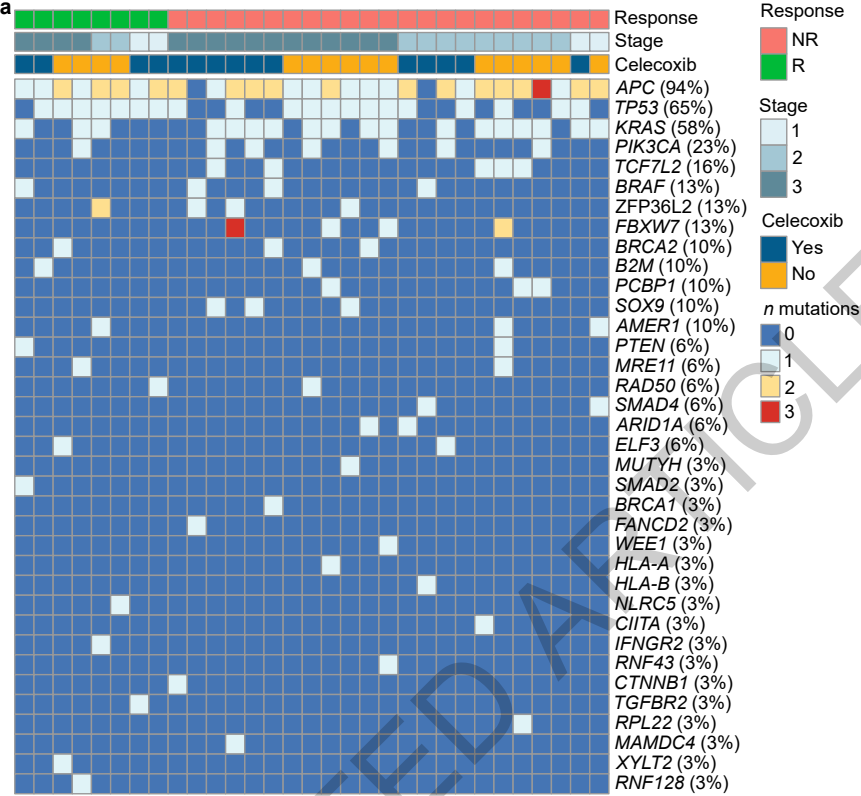
1219 **Extended Data Fig. 7: Cancer-associated fibroblast (CAFs) and myeloid subtypes.**
1220 **a,b,** Heatmap of cancer-associated fibroblasts (**a**) and myeloid (**b**) phenotypes in IMC in pre-treatment
1221 biopsies for responders ($n = 8$) and non-responders ($n = 22$). Response, baseline clinical staging, and TME
1222 classifications are annotated above. **c-f** Comparison of density of CD39 $^+$ CAFs (**a**), PDPN $^+$ CAFs (**b**), HLA-
1223 DR $^+$ monocytes/macrophages (**c**) and CD163 $^+$ monocytes/macrophages (**d**) in IMC in pre-treatment
1224 biopsies for responders ($n = 8$) and non-responders ($n = 22$). **c-f** Distributions were compared with two-
1225 sided Wilcoxon's rank-sum tests. Boxplots represent the median and interquartile range, whiskers
1226 extend from the hinge to the largest value within 1.5 x interquartile range from the hinge.
1227

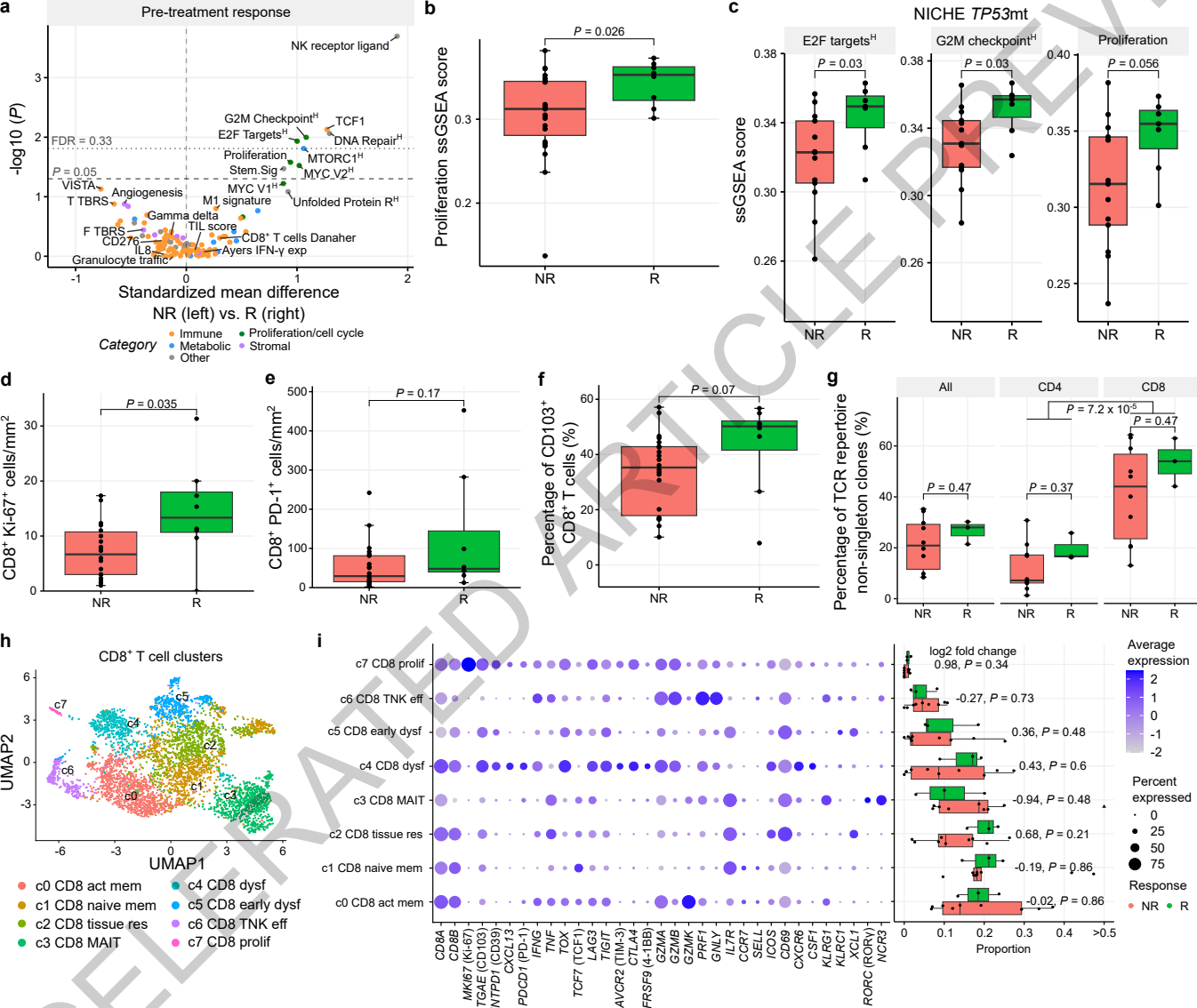
1228 **Extended Data Table 1: Immune related adverse events in all treated patients.**
1229 All adverse events that were deemed at least possibly related to nivolumab and/or ipilimumab are
1230 presented in this table. This is regardless of the possible relationship with celecoxib.
1231

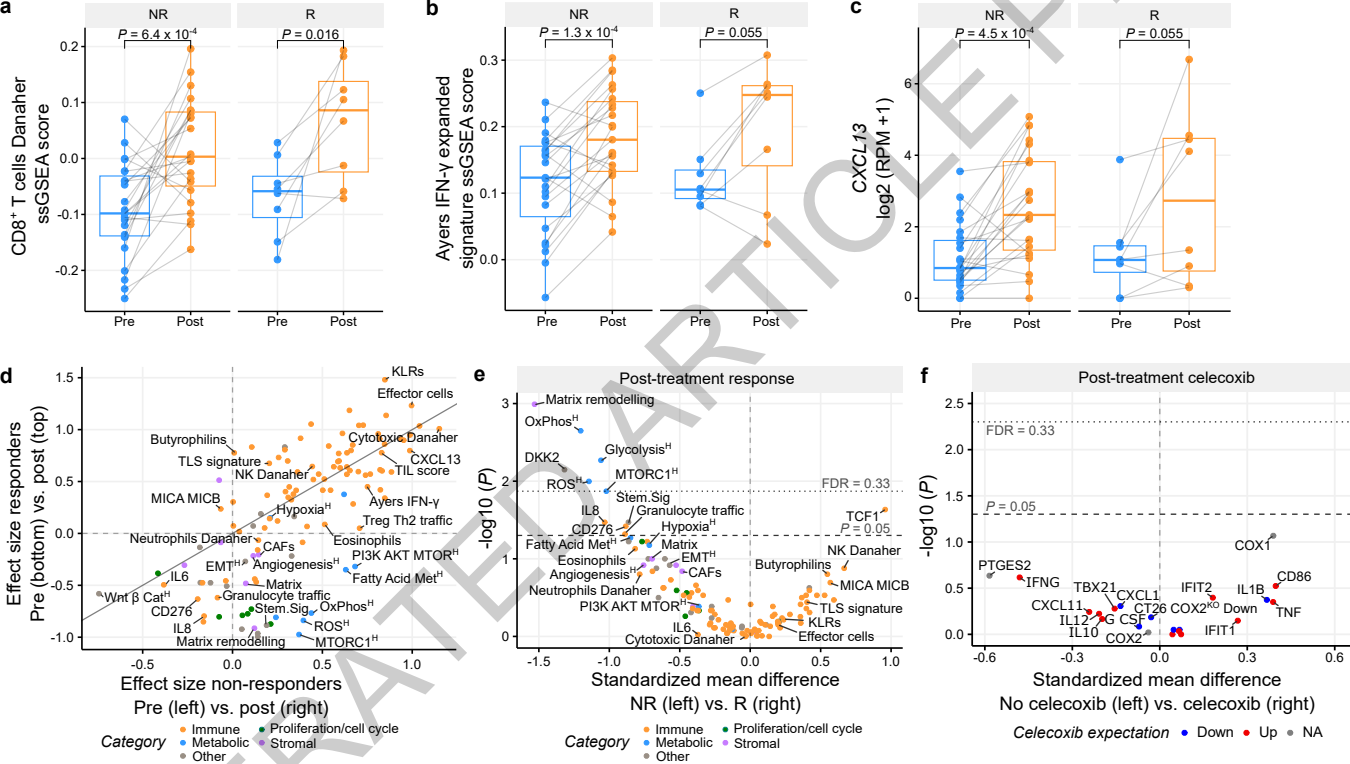
1232 **Extended Data Table 2: Clinical staging and histopathological findings per patient.**
1233 * Patient 86 did not undergo surgery and had a clinical complete response based on radiographic
1234 evaluation and tumour-free biopsies. † Patients 31 and 41 retrospectivey did not meet inclusion criteria
1235 and were excluded from the efficacy analysis; 31 due to liver metastases at baseline and 41 due to
1236 having a mixed adenocarcinoma and neuroendocrine carcinoma (MiNEN). Both patients received
1237 adjuvant chemotherapy due to tumour positive lymph nodes in the resection specimen.
1238 Abbreviations: NR: non-responder; PR: partial responder; MPR: major pathologic response; pCR:
1239 pathological complete response; cCR: clinical complete response
1240

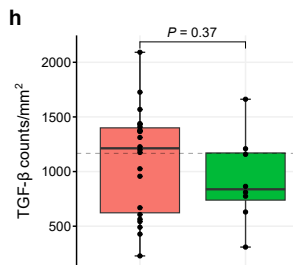
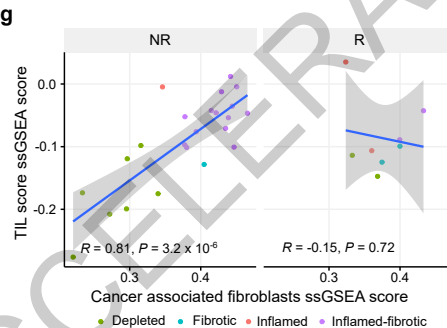
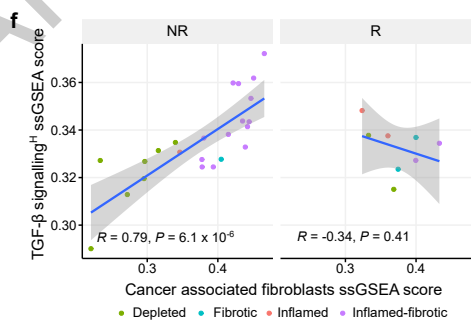
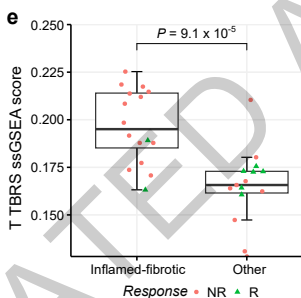
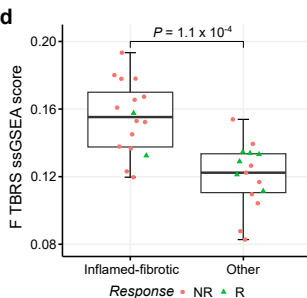
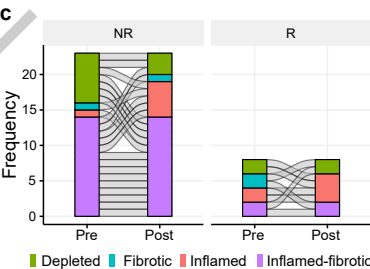
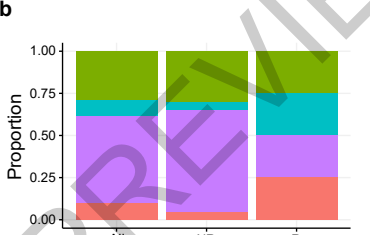
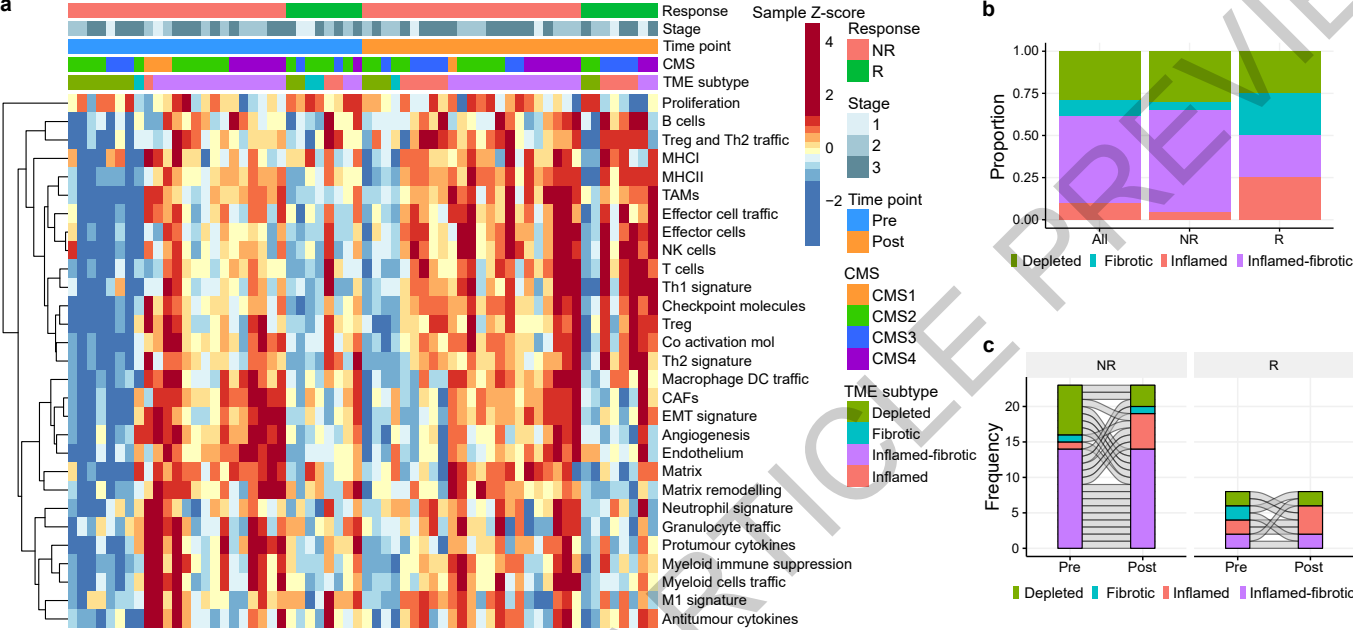
1241 **Extended Data Table 3. TP53 and KRAS mutational status in patients with non-metastatic pMMR colon**
1242 **cancer in NICHE, TCGA and AC-ICAM cohorts.**
1243
1244

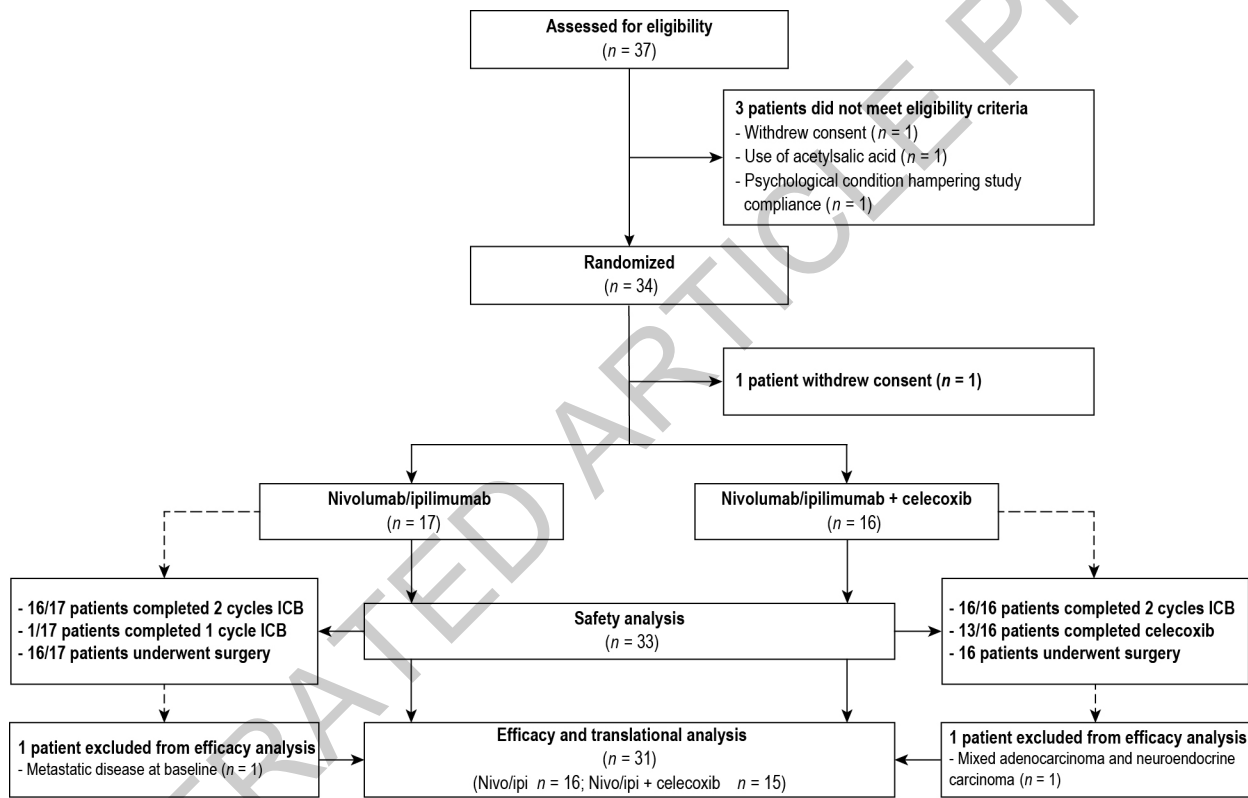




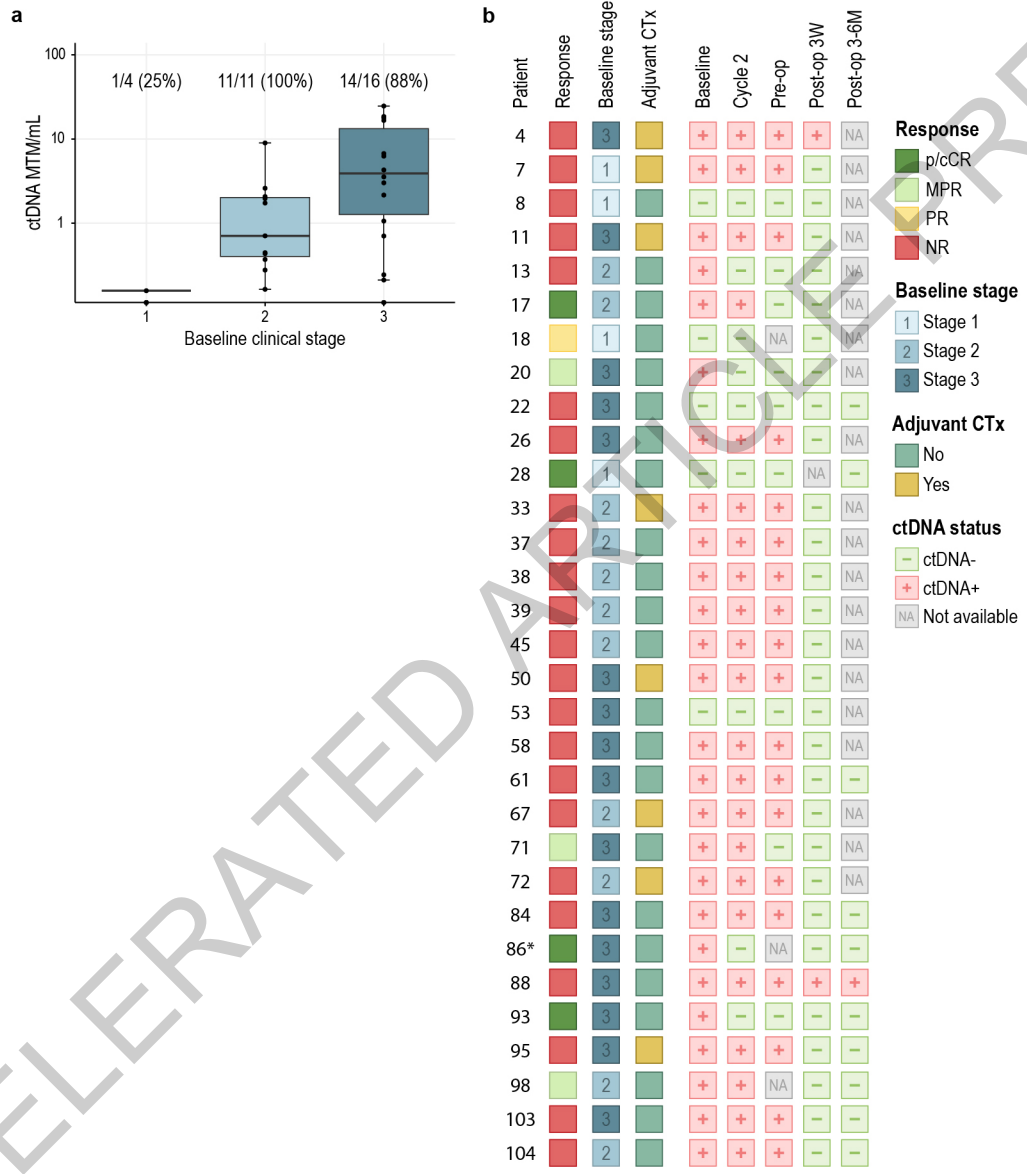




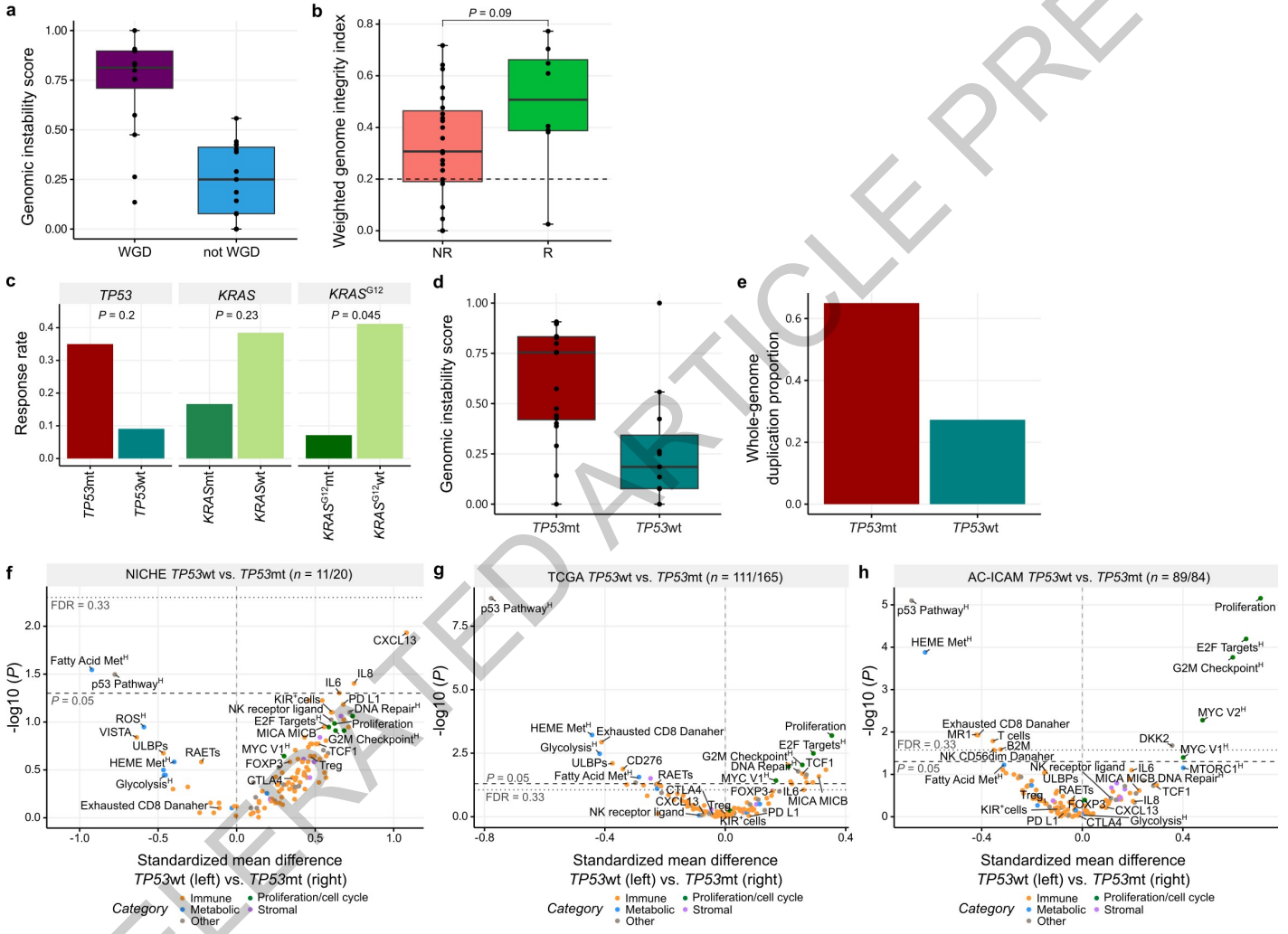




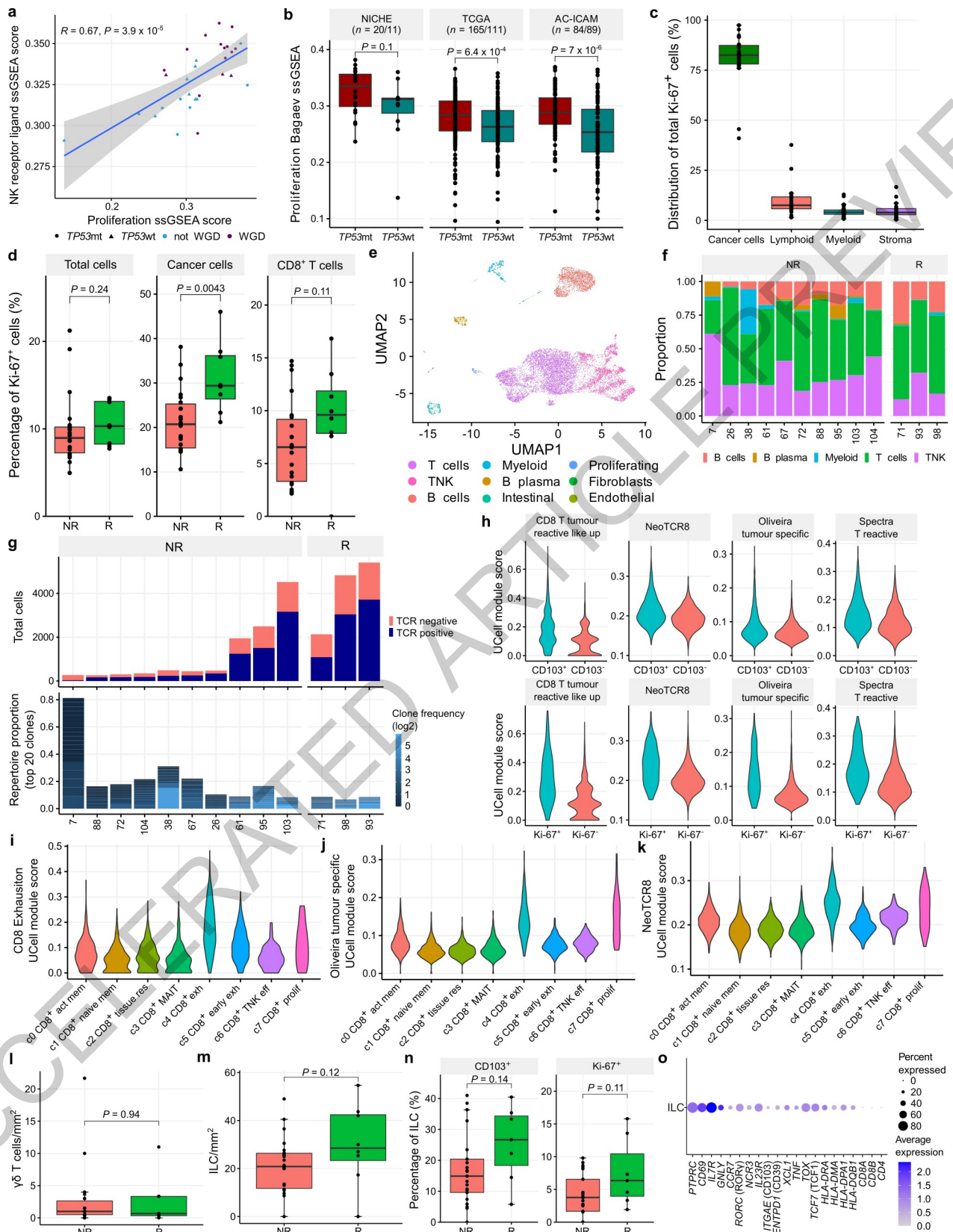
Extended Data Fig. 1



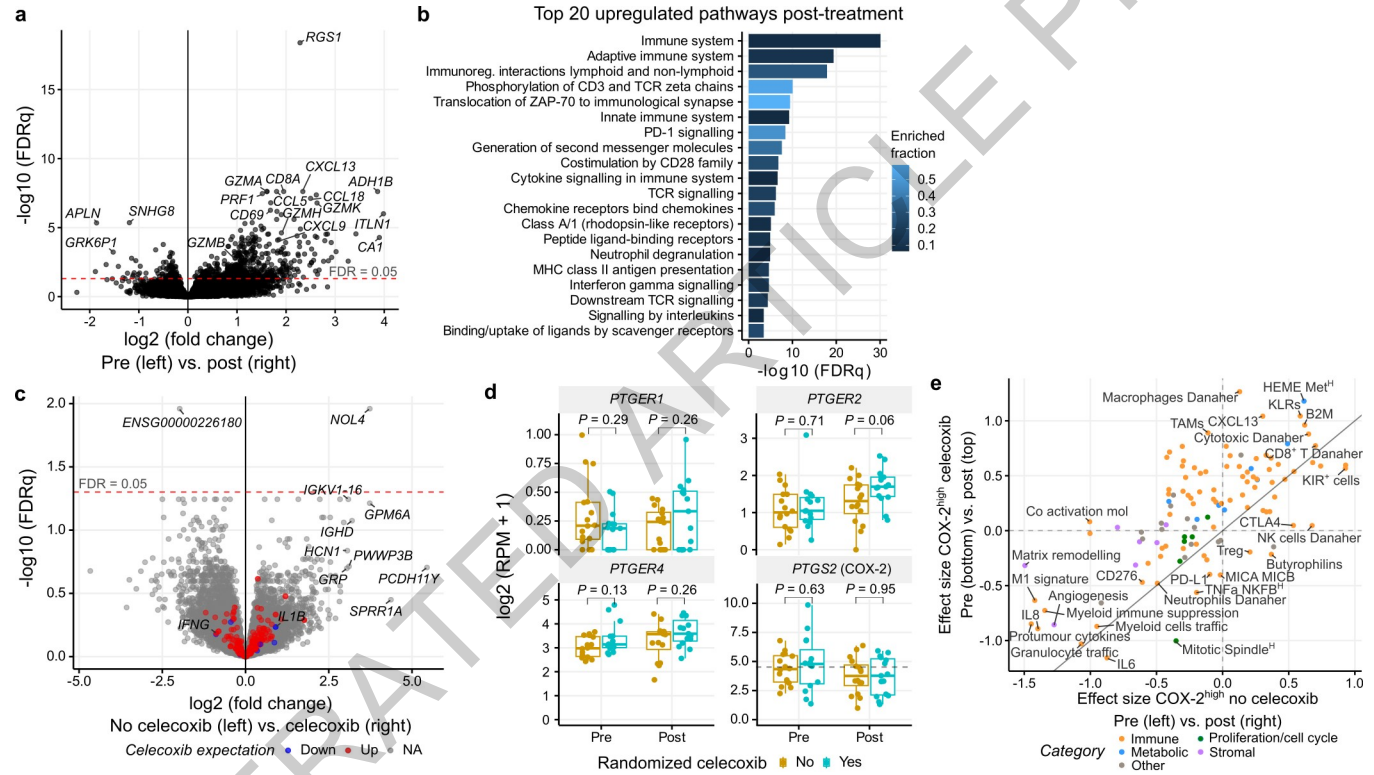
Extended Data Fig. 2



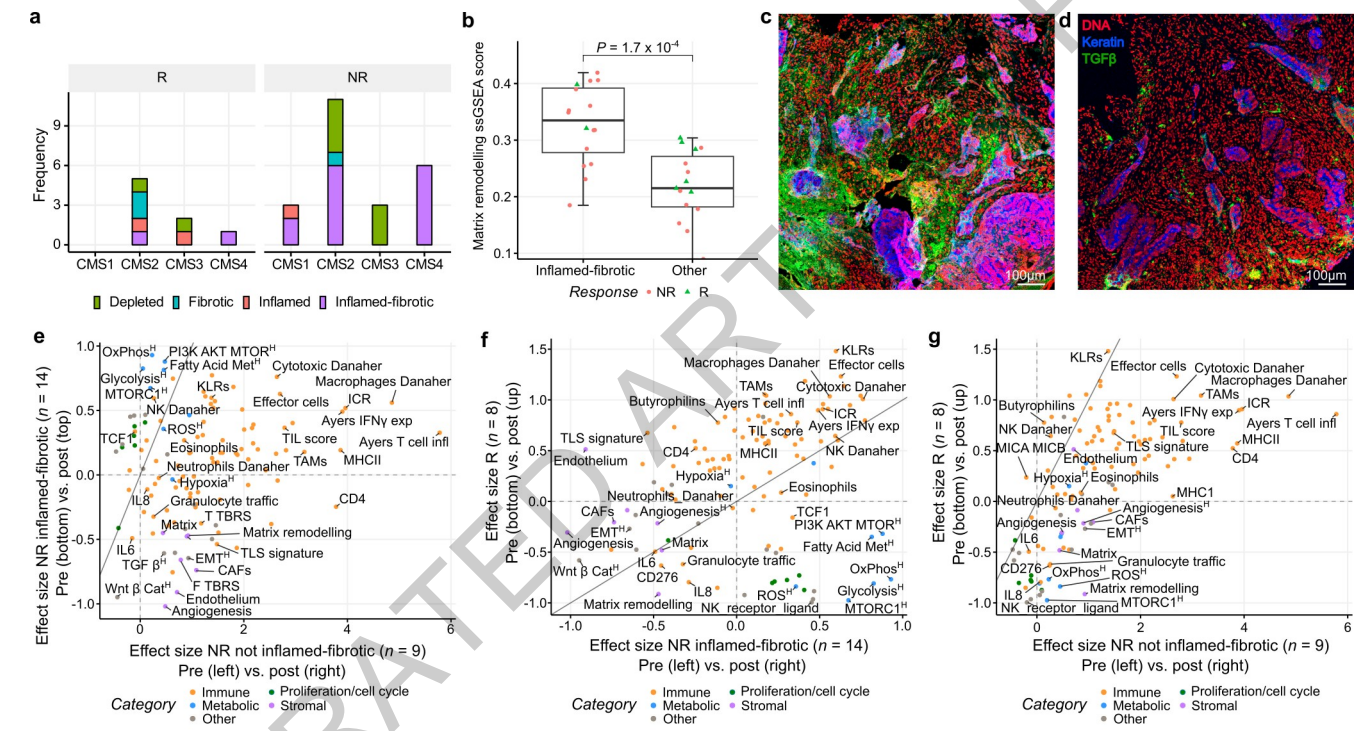
Extended Data Fig. 3



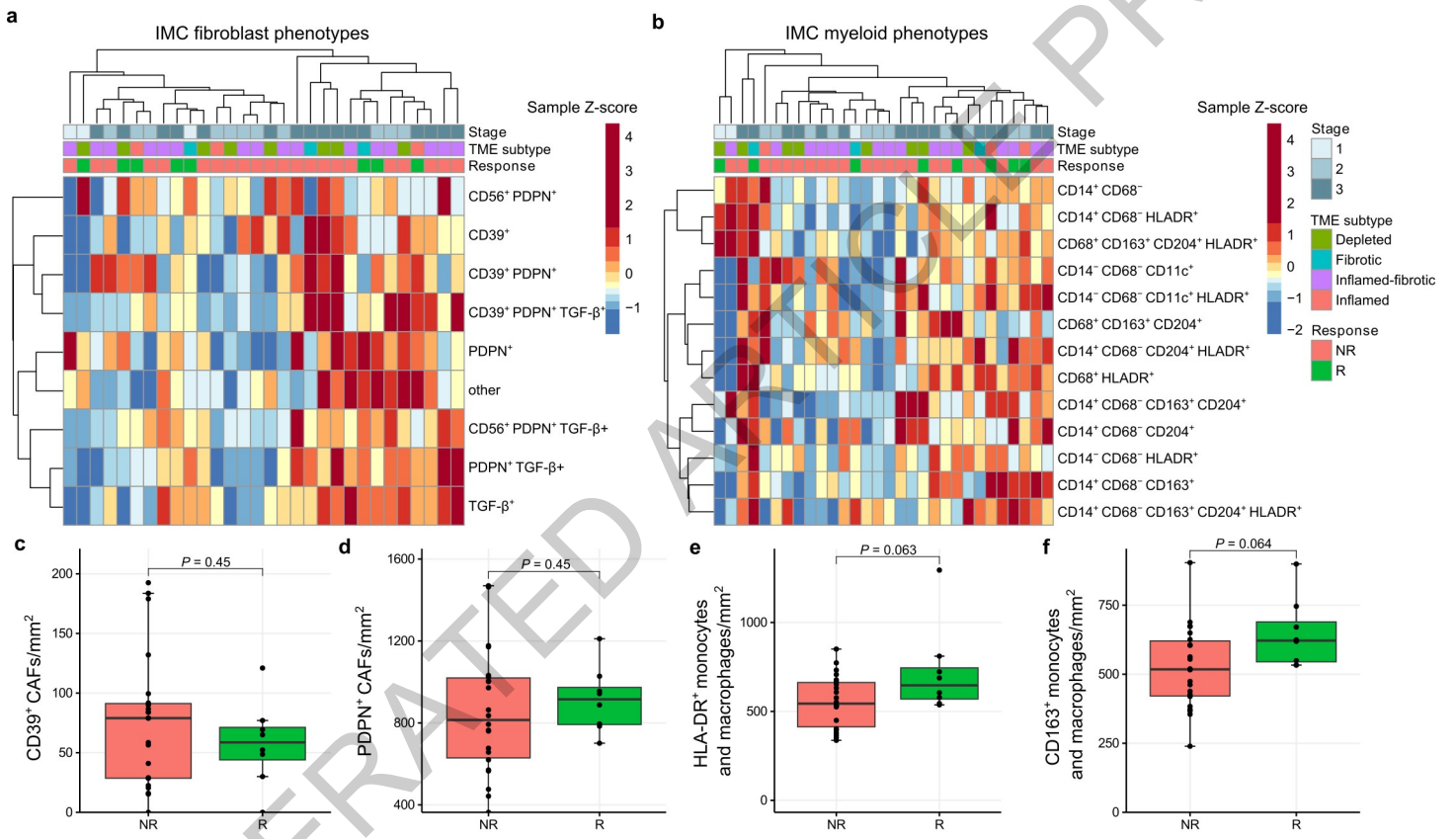
Extended Data Fig. 4



Extended Data Fig. 5



Extended Data Fig. 6



Extended Data Fig. 7

	Patients (n = 33)	
Event – number of patients with event (%)	Grade 1-2	Grade 3
Any grade	22 (67%)	4 (12%)
Infusion-related reaction	8 (24%)	-
Rash, pruritus and/or dry skin	6 (18%)	2 (6%)
Hypothyroidism	6 (18%)	-
Fatigue	3 (9%)	-
Arthritis	2 (6%)	-
Flu like symptoms	2 (6%)	-
Sarcoid like reaction	2 (6%)	-
Arthralgia	1 (3%)	-
Colitis	-	1 (3%)
Diarrhoea	1 (3%)	-
Elevated ALT and/or AST	1 (3%)	-
Hyperthyroidism	1 (3%)	-
Myalgia	1 (3%)	-
Myositis	-	1 (3%)
Parotitis	1 (3%)	-

Extended Data Table 1

Patient	Celecoxib	Pre-treatment clinical TNM staging (stage)	Post-treatment pathological TNM staging (stage)	Post-treatment residual viable tumour (%)	Pathological response category
4	Yes	T3N+ (3)	ypT3N2b (3)	90%	NR
7	No	T2NO (1)	ypT3N1b (3)	90%	NR
8	Yes	T2NO (1)	ypT3N0 (2a)	100%	NR
11	No	T3N+ (3)	ypT3N1a (3)	85%	NR
13	No	T3NO (2a)	ypT3N0 (2a)	100%	NR
17	No	T3NO (2a)	ypTisN0 (pCR)	0%	pCR
18	Yes	T2NO (1)	ypT1N0 (1)	50%	PR
20	Yes	T2N+ (3)	ypT1N0 (1)	1%	MPR
22	Yes	T3N+ (3)	ypT3N0 (2a)	80%	NR
26	No	T3N+ (3)	ypT3N0 (2a)	70%	NR
28	Yes	T2NO (1)	ypT0N0 (pCR)	0%	pCR
33	No	T3NO (2a)	ypT3N1a(m1) (3)	100%	NR
37	Yes	T3NO (2a)	ypT3N0 (2a)	65%	NR
38	Yes	T3NO (2a)	ypT4aN0 (2b)	100%	NR
39	No	T3NO (2a)	ypT3N0 (2a)	97%	NR
45	No	T3NO (2a)	ypT3N0 (2a)	100%	NR
50	No	T4N+ (3)	ypT3N0 (2a)	95%	NR
53	Yes	T3N+ (3)	ypT1N0 (1)	80%	NR
58	No	T3N+ (3)	ypT3N0 (2a)	95%	NR
61	Yes	T3N+ (3)	ypT3N0 (2a)	80%	NR
67	No	T3NO (2a)	ypT3N1a (3)	100%	NR
71	No	T3N+ (3)	ypT0N1b (3)	10%	MPR
72	Yes	T3NO (2a)	ypT3N2a (3)	100%	NR
84	Yes	T3N+ (3)	ypT3N0 (2a)	90%	NR
86*	No	T3N+ (3)	Not evaluable (cCR)	Not evaluable	cCR
88	Yes	T3N+ (3)	ypT3N0 (2a)	100%	NR
93	Yes	T3N+ (3)	ypTisN0 (pCR)	0%	pCR
95	No	T3N+ (3)	ypT3N2a (3)	90%	NR
98	No	T3NO (2a)	ypT1N0 (1)	5%	MPR
103	No	T3N+ (3)	ypT3N0 (2a)	77%	NR
104	Yes	T3NO (2a)	ypT3N0 (2a)	80%	NR
31†	No	T3N+ (3)	ypT3N2b (3)	100%	NR
41†	Yes	T3N+ (3)	ypT3N2b (3)	90%	NR

Extended Data Table 2

Mutational status – number of patients (%)	NICHE (n = 31)	TCGA (n = 287)	AC-ICAM (n = 173)
APCmt	29 (94%)	241 (84%)	130 (75%)
TP53mt	20 (65%)	173 (60%)	84 (49%)
KRASmt	18 (58%)	131 (46%)	69 (40%)
KRAS ^{G12} mt	14 (45%)	92 (32%)	44 (25%)
TP53wt; KRAS ^{G12} wt	4 (13%)	71 (25%)	61 (35%)
TP53wt; KRAS ^{G12} mt	7 (23%)	43 (15%)	28 (16%)
TP53mt; KRAS ^{G12} wt	13 (42%)	124 (43%)	68 (39%)
TP53mt; KRAS ^{G12} mt	7 (23%)	49 (17%)	16 (9%)

Extended Data Table 3

Reporting Summary

Nature Portfolio wishes to improve the reproducibility of the work that we publish. This form provides structure for consistency and transparency in reporting. For further information on Nature Portfolio policies, see our [Editorial Policies](#) and the [Editorial Policy Checklist](#).

Statistics

For all statistical analyses, confirm that the following items are present in the figure legend, table legend, main text, or Methods section.

n/a Confirmed

- The exact sample size (n) for each experimental group/condition, given as a discrete number and unit of measurement
- A statement on whether measurements were taken from distinct samples or whether the same sample was measured repeatedly
- The statistical test(s) used AND whether they are one- or two-sided
Only common tests should be described solely by name; describe more complex techniques in the Methods section.
- A description of all covariates tested
- A description of any assumptions or corrections, such as tests of normality and adjustment for multiple comparisons
- A full description of the statistical parameters including central tendency (e.g. means) or other basic estimates (e.g. regression coefficient) AND variation (e.g. standard deviation) or associated estimates of uncertainty (e.g. confidence intervals)
- For null hypothesis testing, the test statistic (e.g. F , t , r) with confidence intervals, effect sizes, degrees of freedom and P value noted
Give P values as exact values whenever suitable.
- For Bayesian analysis, information on the choice of priors and Markov chain Monte Carlo settings
- For hierarchical and complex designs, identification of the appropriate level for tests and full reporting of outcomes
- Estimates of effect sizes (e.g. Cohen's d , Pearson's r), indicating how they were calculated

Our web collection on [statistics for biologists](#) contains articles on many of the points above.

Software and code

Policy information about [availability of computer code](#)

Data collection	Clinical data from NICHE: TENALEA clinical trial data management system
Data analysis	<ul style="list-style-type: none"> - Analysis of clinical data: R v.4.3.0 , R-studio (build 561), packages: arsenal (v3.6.3), survival (v3.6-4), survminer (v0.4.9) - Analysis of DNA, RNA, IMC data: R v4.2.3, R-studio (build 513), tidyverse (v2.0), ggplot2 (v3.4.2), ggpurr (v0.6.0) pheatmap (v1.0.12). - Analysis of circulating tumor DNA (ctDNA) data: R v4.3.1, packages: stats (v4.3.1), mosaic (v1.9.1) - Imaging Mass Cytometry (IMC): Fluidigm mcd viewer (v1.0.560.6), CellProfiler (v4.2.1), Cytosplore (v2.3.1). - Immunohistochemistry (IHC): HALO v4.0.5107.357 (Indica Labs) with the Indica Labs Multiplex IHC v3.0.3 analysis algorithm - DNA (whole-exome) sequencing: Sarek pipeline (v3.1.2), bwa (v0.7.17), MarkDuplicates (v4.3), GATK BaseRecalibrator (v4.3), Strelka2 (v2.9.10), snpeff (v5.1), ensemblvep (v106.1), vcf2maf (v1.6.22), OncoKB annotator (v3.4.1), ASCAT (v3.0). - RNA sequencing: Hisat2 (v2.2.1), gensum (https://github.com/NKI-GCF/gensum), DESeq2 (v1.38.3), enrichR (v3.2), GSVA (v1.46), geom_smooth (v3.4.2) - scRNA sequencing and TCRsequencing: R v4.2.3, Cell Ranger (v7.1.0); Seurat (v5.2.1); scRepertoire (v2.3.2)

For manuscripts utilizing custom algorithms or software that are central to the research but not yet described in published literature, software must be made available to editors and reviewers. We strongly encourage code deposition in a community repository (e.g. GitHub). See the Nature Portfolio [guidelines for submitting code & software](#) for further information.

Data

Policy information about [availability of data](#)

All manuscripts must include a [data availability statement](#). This statement should provide the following information, where applicable:

- Accession codes, unique identifiers, or web links for publicly available datasets
- A description of any restrictions on data availability
- For clinical datasets or third party data, please ensure that the statement adheres to our [policy](#)

DNA and RNA sequencing data for the NICHE study is deposited in the European Genome-phenome Archive (EGA) under accession number EGAS50000000856. Data is under controlled access according to consent provided by the patients whose samples are used and according to GDPR. Data will be made available for academic use only upon reasonable request and within the confinements of the informed consent and the European Data Protection Regulation. Requests should include project descriptions describing the research goal, privacy, governance and intended use of data, and can be done through <https://ega.nki.nl/>, contacting repository@nki.nl. Requests will be reviewed by the institutional review board of the Netherlands Cancer Institute (NKI) and require signing of a data access agreement with the NKI after approval.

Clinical data from The Cancer Genome Atlas (TCGA) Research Network were obtained from the Clinical data resource Liu et al. 2018 (DOI: 10.1101/j.cell.2018.02.052). TCGA mutational status for CRC was obtained from analysis by Grasso et al. 2018, available as supplementary material (DOI: 10.1158/2159-8290.CD-17-1327). RNAseq data is openly available and was obtained from cBioportal (<https://www.cbioportal.org>), with accession code coadread_tcga_pan_can_atlas_2018. Data for the AC-ICAM CC cohort is openly available and was downloaded from cBioportal (<https://www.cbioportal.org>), with accession code coad_silu_2022.

Research involving human participants, their data, or biological material

Policy information about studies with [human participants or human data](#). See also policy information about [sex, gender \(identity/presentation\), and sexual orientation](#) and [race, ethnicity and racism](#).

Reporting on sex and gender

Patients were included regardless of sex and/or gender. The study protocol did not include any pre-specified sex- or gender-based analyses and no exploratory sex- or gender-based analyses were performed. The biological sex of each patient was collected from the national Personal Records Database (BRP) and used in Table 1 with baseline characteristics of the cohort; the enrolled cohort included 15 females and 18 males.

Reporting on race, ethnicity, or other socially relevant groupings

Race, ethnicity and other socially relevant groupings were not considered in the study design or the analysis and were not reported in the manuscript.

Population characteristics

Patients diagnosed with MMR proficient, previously untreated non-metastatic colon adenocarcinoma who were at least 18 years or older were eligible. Patients were included irrespective of sex and/or gender (included: 55% male, 45% female). There was no age limit and the median age of included patients was 62, ranging from 44 to 77.

All patients had a World Health Organization performance status of 0 or 1 (included: 94% WHO 0 and 6% WHO 1) and adequate hematologic and end-organ function. Key exclusion criteria included signs of obstruction or perforation, prior immunotherapy, active autoimmune disease requiring systemic immunosuppressive treatment, and active concurrent cancer. Baseline characteristics of included patients are presented in Table 1 of the manuscript.

Recruitment

Patients that presented with an initial diagnosis of non-metastatic, resectable colon adenocarcinoma, either at our center or referred from another center, who were potentially eligible for this study were informed about the standard of care and the possibility of participation in the current study and, if relevant, any other studies they were eligible for. Patients deemed eligible for the NICHE study were informed about the aims of this study, the study procedures and study treatment as well as possible adverse events and other hazards to which they may be exposed in case of participation. Interested patients were provided the patient information folder and consent form containing extensive details on the study and study procedures, after which they were given sufficient time to read the materials and decide on participation. Possible inclusion bias may have arisen from the following situations: a) patients with extensive disease (e.g. T4 status) for whom induction or neoadjuvant treatment was deemed necessary were not included in this study since insufficient data were available to justify omission of chemotherapy as an induction treatment). b) Only fit patients with WHO performance status 0 or 1 and no significant comorbidities were included, and while part of the inclusion criteria this is a source of bias in many clinical trials.

Ethics oversight

The study protocol was approved by the institutional review board of the NKI (sponsor) and by the local ethics boards of the participating centers: OLVG and Spaarne Gasthuis. The study was conducted in accordance with the International Conference on Harmonization Guideline for Good Clinical Practice and the principles of the Declaration of Helsinki. All patients provided written informed consent.

Note that full information on the approval of the study protocol must also be provided in the manuscript.

Field-specific reporting

Please select the one below that is the best fit for your research. If you are not sure, read the appropriate sections before making your selection.

Life sciences

Behavioural & social sciences

Ecological, evolutionary & environmental sciences

For a reference copy of the document with all sections, see nature.com/documents/nr-reporting-summary-flat.pdf

Life sciences study design

All studies must disclose on these points even when the disclosure is negative.

Sample size

- The NICHE study is an exploratory, hypothesis-generating study and no formal sample size calculation was performed. The study aimed to treat a total of 30 patients with pMMR colon cancer.
 - Genomic data from the colorectal cancer cohort from The Cancer Genome Atlas Research Network was obtained (n=592) and 287 patients with colon cancer, pathological stage I-III disease and pMMR annotations without POLE mutations were included. RNAseq data was available for 276 of these patients.
 - Genomic data from the colon cancer cohort from the atlas and compass of immune-colon cancer-microbiome interactions (AC-ICAM) was obtained (n=281) and 173 patients with pathological stage I-III disease, pMMR annotations and without POLE mutations were included. RNAseq data was available for all 173 patients.
- The number of external datasets was determined based on availability of openly accessible studies in cBioPortal, with matched RNA and DNA data for early stage pMMR colon cancer samples. Addition of two large external studies was considered sufficient to compare the proportion of genetic alterations and investigate gene expression changes associated with TP53 alterations.

Data exclusions

- All enrolled patients in the NICHE study who received at least 1 cycle of study medication were included in the safety analyses (n=33). Among all treated patients, the patients who met all inclusion criteria at baseline were included in efficacy and translational analyses (n=31).
- For external TCGA and AC-ICAM cohorts, patients with colon cancer, Stage I-III disease, MSS annotations and without POLE mutations, with DNA or RNA data available were included.

Replication

- Replication is not applicable for clinical data, because this study included patients who received neoadjuvant treatment and then underwent surgery, which can only be performed once for an individual. Translational experiments on human samples were not replicated due to limited material.

Randomization

- All patients in NICHE received nivolumab 3 mg/kg on days 1 and 15 plus ipilimumab on day 1. In addition, patients were randomized 1:1 to receive nivolumab/ipilimumab with or without oral celecoxib 200 mg once daily until the day prior to surgery.

Blinding

- Tumour microenvironment subtype classification based on Bagaev et al. signatures was performed blinded to response labels, aided by and distributions of ssGSEA scores for immune and stromal signatures and hierarchical clustering of signature Z-scores. Other experiments were not performed blinded to group allocation, but this was not relevant due to the automation of data collection and analysis across samples.

Reporting for specific materials, systems and methods

We require information from authors about some types of materials, experimental systems and methods used in many studies. Here, indicate whether each material, system or method listed is relevant to your study. If you are not sure if a list item applies to your research, read the appropriate section before selecting a response.

Materials & experimental systems

- | | |
|-------------------------------------|-------------------------------|
| n/a | Involved in the study |
| <input type="checkbox"/> | Antibodies |
| <input checked="" type="checkbox"/> | Eukaryotic cell lines |
| <input checked="" type="checkbox"/> | Palaeontology and archaeology |
| <input checked="" type="checkbox"/> | Animals and other organisms |
| <input type="checkbox"/> | Clinical data |
| <input checked="" type="checkbox"/> | Dual use research of concern |
| <input checked="" type="checkbox"/> | Plants |

Methods

- | | |
|-------------------------------------|------------------------|
| n/a | Involved in the study |
| <input checked="" type="checkbox"/> | ChIP-seq |
| <input checked="" type="checkbox"/> | Flow cytometry |
| <input checked="" type="checkbox"/> | MRI-based neuroimaging |

Antibodies

Antibodies used

Immunohistochemistry (IHC):

- MLH1, Ready-to-Use (=undiluted), M1, 6472966001, LotNo: G07286, G09887, Roche Diagnostics, Tucson, AZ, United States of America
- MSH2, Ready-to-Use (=undiluted), G219-1129, 5269270001, LotNo 2017: 161008B, 1616008C, V0000776, LotNo 2018: V0001229, LotNo 2019: V0001244, V0001272, V0001273, f06034, F1125, f17180. LotNo 2020: f15301, f19415, f29067. 2021 LotNo 2021: g07854, g17138, g32360, h05779, h03163, h05779, h12642, Roche Diagnostics, Tucson, AZ, United States of America
- MSH6, 1/50 dilution, EP49, AC-0047, LotNo: EN020910, EN072101, EN100602, 19060401, 20021305, Abcam, Cambridge, United Kingdom
- PMS2 (used in 2017), 1/20 dilution, clone EP51, M3647, LotNo: 10112572, 10122891, Agilent/DAKO, Santa Clara, California, United States of America
- PMS2 (used in 2018 and thereafter), Ready-to-Use (=undiluted), clone EPR3947, 7604531 LotNo 2018: V0000986, V0001061, V0001217, V0001251, V0001198, V0001253, LotNo 2019: V0001253, F01588M, F060406M, F08243M, F09828M, F05846M, F07456M, LotNo 2020: F16520, F19021, F25056, G03551, G10164 2021: G21216, G10165, G05452, G32555, G33341, G19245, H000178, Roche Diagnostics, Tucson, AZ, United States of America

Imaging Mass Cytometry (IMC):

- IMC antibodies use custom carrier-free formulations with metal conjugations ordered with the respective companies.
- CD4 clone EPR6855, 1/100 dilution, metal: 145 Nd, LotNo: 1014578-6, Abcam, Cambridge, United Kingdom, catalog number ab181724
 - TCRgd clone H41, 1/25 dilution, metal: 148 Nd, LotNo: D3021, Santa Cruz biotechnology, Dallas, United states, catalog number sc-100289
 - Anti-rabbit IgG, polyclonal, 1/100 dilution, metal: 145 Nd, LotNo: GR3215731-15, Abcam, Cambridge, United Kingdom, catalog number ab6701
 - Anti-mouse IgG, polyclonal, 1/100 dilution, metal: 148 Nd, LotNo: GR3300461-1, Abcam, Cambridge, United Kingdom, catalog number ab6708
 - CD8a clone D8A8Y, 1/50 dilution, metal: 146 Nd, LotNo: 2, Cell signaling technology, Danvers, United states, catalog number 81575SF
 - PD-1 clone D4W2J, 1/50 dilution, metal: 160 Gd, LotNo: 1, Cell signaling technology, Danvers, United states, catalog number 63815SF
 - ICOS clone D1K2T(tm), 1/50 dilution, metal: 161 Dy, LotNo: 4, Cell signaling technology, Danvers, United states, catalog number 39740SF
 - CD204 clone J5HTR3, 1/50 dilution, metal: 164 Dy, LotNo: 2518439, Thermo Fisher Scientific, Waltham, United States, catalog number 14-9054-82
 - CD103 clone EPR4166(2), 1/50 dilution, metal: 168 Er, LotNo: GR3399209-2, Abcam, Cambridge, United Kingdom, catalog number ab221210
 - Tbet clone 4B10, 1/50 dilution, metal: 170 Er, LotNo: B298378, Biologend, San Diego, United States, catalog number 644825
 - Caspase clone D4V4B, 1/50 dilution, metal: 172 Yb, LotNo: 25, Cell signaling technology, Danvers, United states, catalog number 74860SF
 - CD163 clone D6U1J, 1/50 dilution, metal: 173 Yb, LotNo: 1, Cell signaling technology, Danvers, United states, catalog number 25121SF
 - HLA-DR clone TAL 1B5, 1/100 dilution, metal: 141 Pr, LotNo: GR3424852-2, Abcam, Cambridge, United Kingdom, catalog number ab176408
 - CD11b clone D6X1N, 1/100 dilution, metal: 144 Nd, LotNo: 1, Cell signaling technology, Danvers, United states, catalog number 23743SF
 - Granzyme B clone D6E9W, 1/100 dilution, metal: 150 Nd, LotNo: 7, Cell signaling technology, Danvers, United states, catalog number 79903SF
 - CD138 clone 5A1E, 1/100 dilution, metal: 155 Gd, LotNo: 1, Cell signaling technology, Danvers, United states, catalog number 94530SF
 - CD39 clone EPR20627, 1/100 dilution, metal: 157 Gd, LotNo: GR3274485-6, Abcam, Cambridge, United Kingdom, catalog number ab236038
 - VISTA clone D1L2G(TM), 1/100 dilution, metal: 158 Gd, LotNo: 7, Cell signaling technology, Danvers, United states, catalog number 56548SF
 - CD14 clone D7A2T, 1/100 dilution, metal: 163 Dy, LotNo: 2, Cell signaling technology, Danvers, United states, catalog number 43878SF
 - CD56 clone E7X9M, 1/100 dilution, metal: 167 Er, LotNo: 2, Cell signaling technology, Danvers, United states, catalog number 88856SF
 - CD7 clone EPR4242, 1/100 dilution, metal: 174 Yb, LotNo: GR3424737-2, Abcam, Cambridge, United Kingdom, catalog number ab230834
 - CD11c clone EP1347Y, 1/100 dilution, metal: 176 Yb, LotNo: GR3357092-17, Abcam, Cambridge, United Kingdom, catalog number ab216655
 - CD45 clone D9M8I, 1/50 dilution, metal: 149 Sm, LotNo: 12, Cell signaling technology, Danvers, United states, catalog number 47937SF
 - CD3 clone EP449E, 1/50 dilution, metal: 153 Eu, LotNo: GR3418069-6, Abcam, Cambridge, United Kingdom, catalog number ab271850
 - PD-L1 clone E1L3N(R), 1/50 dilution, metal: 156 Gd, LotNo: 2, Cell signaling technology, Danvers, United states, catalog number 85164SF
 - FOXP3 clone D608R, 1/50 dilution, metal: 159 Tb, LotNo: 2, Cell signaling technology, Danvers, United states, catalog number 72338SF
 - CD27 clone EPR8569, 1/50 dilution, metal: 175 Lu, LotNo: GR3446729-2, Abcam, Cambridge, United Kingdom, catalog number ab192336
 - Vimentin clone D21H3, 1/50 dilution, metal: 194 Pt, LotNo: 1, Cell signaling technology, Danvers, United states, catalog number 46173SF
 - Keratin clone C11, 1/50 dilution, metal: 198 Pt, LotNo: 2, Cell signaling technology, Danvers, United states, catalog number 17171SF
 - Keratin clone AE1/AE3, 1/50 dilution, metal: 198 Pt, LotNo: B302316, Biologend, San Diego, United states, catalog number 914204
 - TGF β clone TB21, 1/100 dilution, metal: 89Y, LotNo: 157850, Cell signaling technology, Danvers, United states, catalog number MA5-16949
 - CD20 clone H1, 1/100 dilution, metal: 142 Nd, LotNo: 1209781, BD Biosciences, Franklin Lakes, United states, catalog number 555677
 - CD68 clone D4B9C, 1/100 dilution, metal: 143 Nd, LotNo: 2, Cell signaling technology, Danvers, United states, catalog number 26042SF
 - CD31 clone 89C2, 1/100 dilution, metal: 147 Sm, LotNo: 1, Cell signaling technology, Danvers, United states, catalog number 85873SF
 - CD57 clone HNK-1 / Leu-7, 1/100 dilution, metal: 151 Eu, LotNo: GR3373313, Abcam, Cambridge, United Kingdom, catalog number ab212403
 - Ki-67 clone 8D5, 1/100 dilution, metal: 152 Sm, LotNo: 11, Cell signaling technology, Danvers, United states, catalog number 62548SF
 - IgG1 clone EPR4417, 1/100 dilution, metal: 154 Sm, Abcam, Cambridge, United Kingdom, catalog number ab232544
 - IDO clone D5J4E(TM), 1/100 dilution, metal: 162 Dy, LotNo: 7, Cell signaling technology, Danvers, United states, catalog number 91473SF
 - CD45RO clone UCHL1, 1/100 dilution, metal: 165 Ho, LotNo: 1, Cell signaling technology, Danvers, United states, catalog number 36282SF
 - D2-40 clone D2-40, 1/100 dilution, metal: 166 Er, LotNo: B316467,

Biolegend, San Diego, United states, catalog number 916606

- CD38 clone EPR4106, 1/100 dilution, metal: 169 Tm, LotNo: GR3378690-1, Abcam, Cambridge, United Kingdom, catalog number ab226034
- CD15 clone MC480, 1/100 dilution, metal: 171 Yb, LotNo: 5, Cell signaling technology, Danvers, United states, catalog number 74180SF
- Bcatenin clone D10A8, 1/100 dilution, metal: 196 Pt, LotNo: 1, Cell signaling technology, Danvers, United states, catalog number 84441SF
- Histone H3 clone D1H2, 1/50 dilution, metal: 209 Bi, LotNo: 1, Cell signaling technology, Danvers, United states, catalog number 60932SF

scRNAseq hashing and protein markers:

- TotalSeq-C anti-human hashtag antibodies (clones LNH-94 and 2M2, numbers 1–13; final concentration 1µg/mL, BioLegend), catalog numbers 394661, 394663, 394665, 394667, 394669, 394671, 394673, 394675, 394677, 394679, 328941, 394683, 394685
- anti-CD45-PerCP-Cy5.5, clone HI30, 1/50 dilution, Invitrogen, catalog number 45-0459-42
- PD-1, clone EH12-EH7, 1/1000 dilution, TotalSeq-C, BioLegend, catalog number 329902
- CD39, clone A1, 1/1000 dilution, TotalSeq-C, BioLegend, catalog number 328237
- CD137, clone 4B4-1, 1/5000 dilution, TotalSeq-C, BioLegend, catalog number 309839
- CD8, clone SK1, 1/5000 dilution, TotalSeq-C, BioLegend, catalog number 344753
- CD4, clone RPA-T4, 1/2500 dilution, TotalSeq-C, BioLegend, catalog number 300567

Validation

For MLH1, MSH2, MSH6, and PMS2, IHC protocols have been developed and validated under standard operating procedures in a certified pathology lab (EN ISO15189, M258). Each new antibody lot is validated by testing multiple dilutions and evaluation by a pathologist using a standardized method, using positive control tissues suitable for the antibody (images and protocol details available upon request). Antibodies were validated as described on the manufacturer's websites.

All IMC antibodies have been selected based on extensive validation for use in immunohistochemistry on FFPE tissue by the respective companies. All antibodies are tested in house on FFPE tonsil and colon tissue and staining patterns were compared to company datasheets and reported literature. After metal conjugation, the staining patterns of each antibody are once again validated by IHC and compared to staining prior to conjugation and reported literature. Furthermore, for each antibody, colocalization with expected other markers was confirmed by IMC.

All scRNAseq antibodies were tested for human reactivity, and validated for proteogenomics by the manufacturer. Antibodies are quality control tested by immunofluorescent staining with flow cytometric analysis and the oligomer sequences are confirmed by sequencing. Anti-CD45 clone HI30 has been validated for flow cytometry applications "This HI30 antibody has been pre-titrated and tested by flow cytometric analysis of normal human peripheral blood cells".

Roche Diagnostics antibodies are validated for human reactivity, with visual inspection of CRC and tonsil material stainings, measuring specific and background staining intensities, are free of particulate matter and turbidity. Agilent antibodies are validated by IHC with system level controls to ensure the validity of the staining procedure. Abcam antibodies undergo biophysical quality controls with liquid mass chromatography mass spectrometry and high-performance liquid chromatography and are validated for applications with positive and negative cell lines and tissues, and antibodies are often knockout validated for specificity. Cell signaling technology antibodies are validated for IHC: "Western blot analysis is performed to demonstrate specific bands of the appropriate molecular weight(s), with minimal cross-reacting bands. Paraffin-embedded cell pellets of known target expression levels are used to verify target specificity. Antibody performance is assessed in relevant mouse models of cancer. Xenografts generated from cell lines with known target expression levels help verify target specificity. Human cancer tissue arrays are used to demonstrate antibody performance over a broad spectrum of tissue types. Staining on fresh frozen tissues is performed when appropriate. Tissue sections and cell pellets are subjected to phosphatase treatment to verify target phospho-specificity. The use of blocking peptides verifies specificity and rules out Fc-mediated binding and other non-specific staining. Thorough lot testing ensures the reproducibility necessary for accurate IHC results. Dilutions and protocols are predetermined and specified; control reagents are also available". All antibodies on the Thermo Fisher Scientific website that have undergone and passed the advanced verification testing are identified with an "Advanced Verification" badge. Advanced verification is additional testing that verifies that an antibody will bind to the correct target. BD Biosciences antibodies: "Our product development process includes testing on a combination of primary cells, cell lines and/or transfected cell models with relevant controls using multiple immunoassays to ensure biological accuracy. We also perform multiplexing with additional antibodies to interrogate antibody staining in multiple cell populations."

Clinical data

Policy information about [clinical studies](#)

All manuscripts should comply with the ICMJE [guidelines for publication of clinical research](#) and a completed [CONSORT checklist](#) must be included with all submissions.

Clinical trial registration

[ClinicalTrials.gov](#), NCT03026140

Study protocol

The study protocol is provided as supplementary information.

Data collection

Clinical data, including data regarding adverse events, were collected from time of signing informed consent until 100 days after the last administration of study drugs. These data were collected through patient consultation in the outpatient clinic of the Netherlands Cancer Institute. Outcome data and long-term survival are collected until five years after initial diagnosis. These long-term data are collected through the outpatient clinic, by telephone consultation or through telemedicine. The first patient was enrolled on June 29th, 2017 and the last patient on July 26th, 2021.

Outcomes

The primary outcome was to determine safety and feasibility. Patients were closely monitored for adverse events until 100 days after the last dose of immunotherapy and were graded according to the Common Terminology Criteria for Adverse Events (CTCAE) version 4.03. Safety was evaluated on the basis of adverse events and serious adverse events. Feasibility was evaluated by treatment-related adverse events leading to surgical delay past the predefined 6 weeks after study enrollment.

Secondary and translational endpoints included efficacy evaluated by histopathologic response and clinical outcomes as well as assessment of associations between responses and genomic, transcriptomic and imaging mass cytometry findings of the tumor microenvironment.

Plants

Seed stocks

Not applicable

Novel plant genotypes

Not applicable

Authentication

Not applicable